



OPEN ACCESS

Edited by:

Edward A. Johnson,
University of Calgary, Canada

Reviewed by:

Tom Jilbert,
University of Helsinki, Finland
Xiaole Sun,
Stockholm University, Sweden

***Correspondence:**

Jorien E. Vonk
j.e.vonk@vu.nl
Kirsi H. Keskitalo
k.h.keskitalo@vu.nl

†ORCID:

Kirsi H. Keskitalo
orcid.org/0000-0001-5793-5083
Lisa Bröder
orcid.org/0000-0002-5454-7883
Sarah Shakil
orcid.org/0000-0002-8877-4830
Scott Zolkos
orcid.org/0000-0001-9945-6945
Suzanne E. Tank
orcid.org/0000-0002-5371-6577
Bart E. van Dongen
orcid.org/0000-0003-1189-142X
Tommaso Tesi
orcid.org/0000-0002-1686-3375
Negar Haghipour
orcid.org/0000-0001-8223-0536
Timothy I. Eglinton
orcid.org/0000-0001-5060-2155
Jorien E. Vonk
orcid.org/0000-0002-1206-5878

Specialty section:

This article was submitted to
Biogeoscience,
a section of the journal
Frontiers in Earth Science

Received: 16 December 2020

Accepted: 01 March 2021

Published: 29 March 2021

Citation:

Keskitalo KH, Bröder L, Shakil S,
Zolkos S, Tank SE, van Dongen BE,
Tesi T, Haghipour N, Eglinton TI,
Kokelj SV and Vonk JE (2021)
Downstream Evolution of Particulate
Organic Matter Composition From
Permafrost Thaw Slumps.
Front. Earth Sci. 9:642675.
doi: 10.3389/feart.2021.642675

Downstream Evolution of Particulate Organic Matter Composition From Permafrost Thaw Slumps

Kirsi H. Keskitalo^{1*†}, Lisa Bröder^{1,2†}, Sarah Shakil^{3†}, Scott Zolkos^{3,4†}, Suzanne E. Tank^{3†}, Bart E. van Dongen^{5†}, Tommaso Tesi^{6†}, Negar Haghipour^{2,7†}, Timothy I. Eglinton^{2†}, Steven V. Kokelj⁸ and Jorien E. Vonk^{1*†}

¹ Department of Earth Sciences, Vrije Universiteit Amsterdam, Amsterdam, Netherlands, ² Department of Earth Sciences, Swiss Federal Institute of Technology, Zurich, Switzerland, ³ Department of Biological Sciences, University of Alberta, Edmonton, AB, Canada, ⁴ Woodwell Climate Research Center, Falmouth, MA, United States, ⁵ Williamson Research Centre for Molecular Environmental Science, Department of Earth and Environmental Sciences, The University of Manchester, Manchester, United Kingdom, ⁶ National Research Council, Institute of Polar Sciences, Bologna, Italy, ⁷ Laboratory of Ion Beam Physics, Swiss Federal Institute of Technology, Zurich, Switzerland, ⁸ Northwest Territories Geological Survey, Yellowknife, NT, Canada

Permafrost soils, which store almost half of the global belowground organic carbon (OC), are susceptible to thaw upon climate warming. On the Peel Plateau of northwestern Canada, the number and size of retrogressive thaw slumps (RTS) has increased in recent decades due to rising temperatures and higher precipitation. These RTS features caused by the rapid thaw of ice-rich permafrost release organic matter dominantly as particulate organic carbon (POC) to the stream network. In this study, we sampled POC and streambank sediments along a fluvial transect (~12 km) downstream from two RTS features and assessed the composition and degradation status of the mobilized permafrost OC. We found that RTS features add old, Pleistocene-aged permafrost POC to the stream system that is traceable kilometers downstream. The POC released consists mainly of recalcitrant compounds that persists within stream networks, whereas labile compounds originate from the active layer and appear to largely degrade within the scar zone of the RTS feature. Thermokarst on the Peel Plateau is likely to intensify in the future, but our data suggest that most of the permafrost OC released is not readily degradable within the stream system and thus may have little potential for atmospheric evasion. Possibilities for the recalcitrant OC to degrade over decadal to millennial time scales while being transported via larger river networks, and within the marine environment, do however, still exist. These findings add to our understanding of the vulnerable Arctic landscapes and how they may interact with the global climate.

Keywords: Arctic, climate, carbon, lipid biomarkers, Peel Plateau, permafrost, pyrolysis-GCMS, degradation

INTRODUCTION

Air temperatures in the Arctic have been rising twice as fast as the global average during the last decades (IPCC, 2013). Permafrost (i.e., perennially frozen ground) underlain soils in the northern circumpolar region store $1,300 \pm 200$ Pg of organic carbon (OC), about twice the amount of carbon currently present in the atmosphere (Hugelius et al., 2014; Schuur et al., 2015). The accelerated

thaw of permafrost, releases OC that has been sequestered over the Last Glacial period to the active carbon cycle (Strauss et al., 2017; Biskaborn et al., 2019). The possible re-mineralization of permafrost OC and release to the atmosphere as greenhouse gases may enhance warming of the climate (Zimov et al., 2006; Schuur et al., 2015; Meredith et al., 2019).

Aside from gradual permafrost thaw that establishes itself through an increase in active layer thaw depth, abruptly thawing permafrost sites at locations with high ground-ice content are becoming more common (Segal et al., 2016; Farquharson et al., 2019). These thermokarst features (e.g., retrogressive thaw slumps, eroding coastlines) form through rapid degradation of ice-rich permafrost (Vonk et al., 2012; Kokelj and Jorgenson, 2013; Schuur et al., 2015). Estimates suggest that thermokarst-susceptible landscapes hold about half of the total OC pool of the Arctic, while only covering 20% of the Arctic permafrost region (Olefelt et al., 2016; Turetsky et al., 2020).

In the Canadian Arctic, the occurrence of thermokarst features is particularly high in ice-marginal terrain deposited by the Laurentide Ice Sheet (LIS) that covered the landscape during the Last Glacial period (Kokelj et al., 2017b). In one of these ice-marginal regions, Banks Island, the number of new retrogressive thaw slump (RTS) features increased 60-fold between 1984 and 2015 (Lewkowicz and Way, 2019). On the Peel Plateau, another ice-marginal glaciated landscape (Kokelj et al., 2017b), abruptly thawing RTS features have increased in size and number in the past decades due to rising temperatures and increased precipitation (Kokelj et al., 2015; Segal et al., 2016). Retreat rates for RTS headwalls varied from 7.2 to 26.7 m yr⁻¹ (on a 20-year average) between 1990 and 2010, but were as high as 60 m yr⁻¹ for some RTS features (Lacelle et al., 2015). Intensifying thermokarst increases the thickness and diversity of permafrost material types thawed (Kokelj et al., 2020, in review), and the hydrochemical effects of these types of abrupt thaw events are known to cascade across entire watersheds (Kokelj et al., 2017b, 2020 in review; Vonk et al., 2015a).

Streams affected by RTS features and active layer detachment slides increase slope sediment yields by orders of magnitude (Kokelj et al., 2013; Rudy et al., 2017; Shakil et al., 2020). Based on yearly (2016–2017) volume loss from headwall retreat of two of the larger RTS features on the Peel Plateau, in the Stony Creek watershed (FM2 and FM3), their combined sediment yields were estimated to be $0.9 \times 10^5 \text{ m}^3 \text{ km}^2 \text{ yr}^{-1}$ (van der Sluijs et al., 2018; Shakil et al., 2020). The high amounts of sediment and OC released from RTS features feed into headwater catchments, potentially affecting entire watersheds (Kokelj et al., 2013, 2017b, 2020 in review).

There are still large uncertainties in the current knowledge on the characteristics of POC and its decomposability, especially in ice-rich glacial terrain where climate history, paleoecology and parent materials may vary (Shakil et al., 2020). Here, we address these knowledge gaps by characterizing the composition and degradation status of POC released from two active RTS sites (FM3 and FM2) over a 12 km-long downstream transect. Along the transect and within the RTS features feeding it, we quantify concentrations of POC, dissolved organic carbon (DOC) and recently deposited sedimentary OC, and use carbon

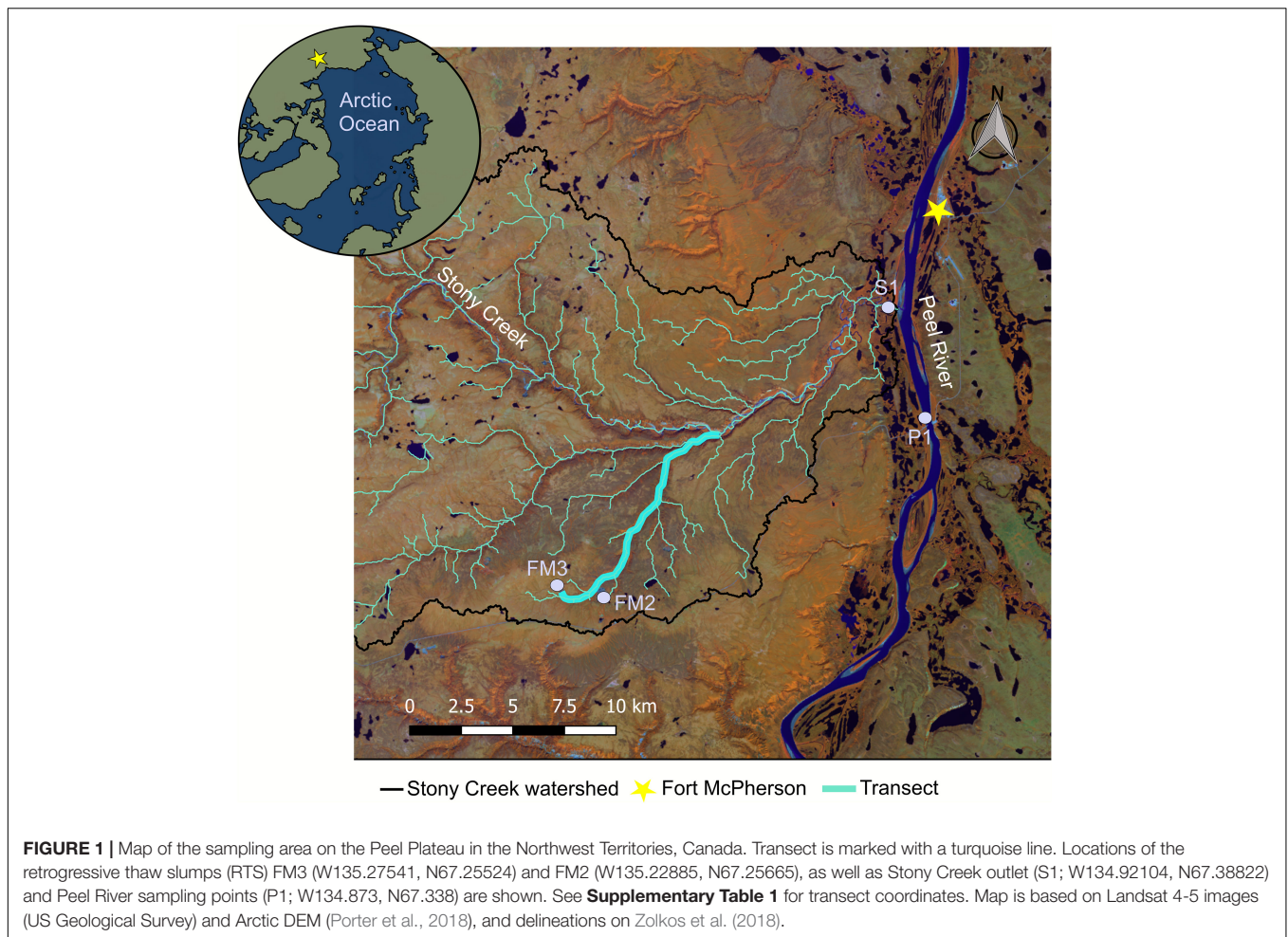
isotopes ($\delta^{13}\text{C}$ and $\Delta^{14}\text{C}$) as diagnostic tools to characterize OC composition. Furthermore, we couple POC and sedimentary OC to the physical properties of the released sediment using grain size distributions and mineral-specific surface area analyses. To trace sources of water along the transect, we use stable water isotopes ($\delta^{18}\text{O}$ and $\delta^2\text{H}$). Additionally, we employ lipid biomarkers (*n*-alkanes and *n*-alkanoic acids) and pyrolysis-gas chromatography-mass spectrometry (py-GCMS) to characterize composition of particulate organic matter on a (macro)molecular level, and assess the degradation status of organic matter on the Peel Plateau. This level of compositional analysis of particulate organic matter released from RTS features has so far not been applied, and helps to discern the possible climate impacts of downstream transport of particulate organic matter. As glacially conditioned permafrost landscapes, such as the Peel Plateau, are amongst the most climate sensitive environments on the planet, it is crucial to understand the vulnerability of the mobilized OC, and how readily it may re-mineralize to the atmosphere as greenhouse gases.

MATERIALS AND METHODS

Study Area

The Peel Plateau is located in the Northwest Territories of Canada and covers an area of 24,000 km² (Kokelj et al., 2017a; **Figure 1**). It is characterized by tundra at the higher elevations in the west and by spruce forests, dominated by black spruce, alder, willow and dwarf birch in the understory, in valleys and lower elevations in the east (O'Neill et al., 2015). Based on historical data from 1981 to 2010, average daily temperatures during the summer months (June–August) range between 11.8 and 15.2°C (measured at the closest weather station at Fort McPherson), while daily average for the coldest month (January) is -31.1°C (Environment Canada, 2019). For the same time period, average annual precipitation is 298 mm of which 152.5 mm falls as snow (Environment Canada, 2019). Precipitation is increasing in the area and is contributing to greater development and activity of retrogressive thaw slumps (Kokelj et al., 2015). The study area was covered by the LIS during the Last Glacial period (ca. 18,500–15,000 yr BP, Zazula et al., 2009; Lacelle et al., 2013), and the landscape is comprised mostly of tills, glaciofluvial, lacustrine and colluvial deposits consisting of clay, silt, sand and coarser materials (Duk-Rodkin and Hughes, 1992; Dyke et al., 2002).

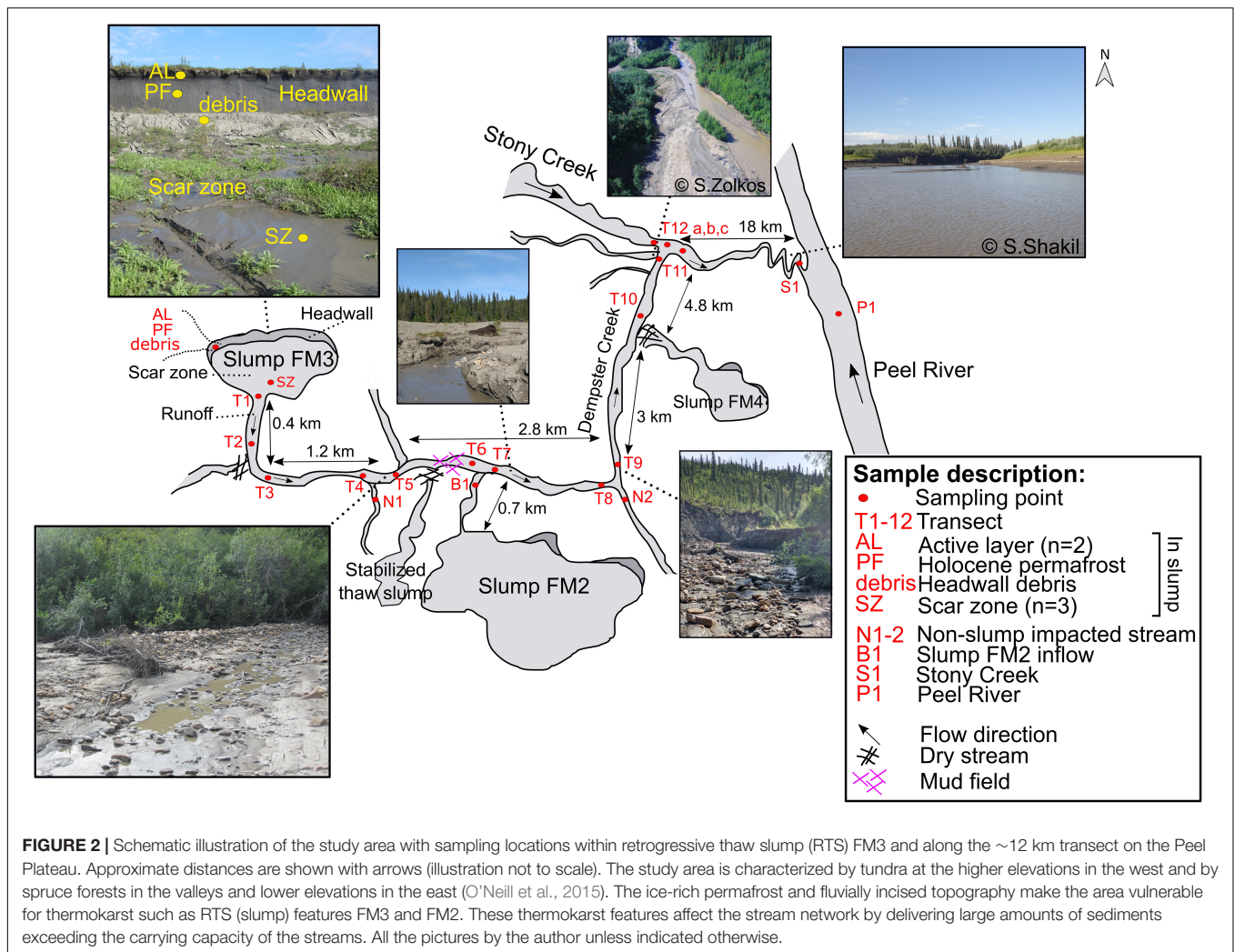
The area is underlain by ice-rich (~50% by volume), Pleistocene-aged permafrost (Lacelle et al., 2013). This glacially conditioned landscape with high ice content permafrost in combination with a fluvially incised topography, has produced a terrain that is highly susceptible to the development of RTS features (Kokelj et al., 2017b). These features develop by ablation of ground ice, destabilizing permafrost slopes and mobilizing previously frozen materials downslope, making sediment and soluble materials available for transport by surface runoff and streams. The RTS features are often polycyclic regarding their thaw activity: rapid melt of ground ice and slump development is followed by a stabilization phase when thawed materials accumulate on the slope, preserving ice underneath. Slumping is



often rejuvenated when physical or thermal erosion destabilizes the vegetated scar zone (Kokelj et al., 2015; Lacelle et al., 2019). They can remain active for decades and continue to deliver large amounts of sediment and associated carbon to stream and river networks downstream (Kokelj et al., 2013). The Peel Plateau has several mega RTS features which are characterized by deep headwalls (up to 25 m), large thaw-impacted areas (>5 ha) and long debris tongue deposits that link thawing slopes with downstream environments (Kokelj et al., 2013, 2015, 2020 in review). Soil and permafrost stratigraphy in the region consists of three distinctive layers: (1) A lower unit of Pleistocene-aged, ice- and mineral-rich sediments, that did not previously thaw (Lacelle et al., 2019); (2) A middle unit 1 to 3 m in thickness of relatively organic-rich substrate compared to the underlying ice-rich tills which was thawed during a warm period in the early Holocene (Lacelle et al., 2019); (3) A modern active layer. These headwall characteristics have been previously described more in detail in Lacelle et al. (2013, 2019) and Malone et al. (2013). Unlike from abrupt thaw sites in Siberia and Alaska (e.g., Abbott et al., 2015; Mann et al., 2015; Vonk et al., 2015b; Textor et al., 2019), DOC release from RTS features on the Peel Plateau is not significantly higher, and in places even lower, than that in unimpacted streams (i.e., in streams not influenced

by RTS features) (Littlefair et al., 2017). Yet, DOC has been shown to be highly biolabile (Littlefair et al., 2017; Littlefair and Tank, 2018). Release of POC from RTS features is orders of magnitude higher than that of DOC, and it differs in its bulk geochemical composition relative to DOC (Shakil et al., 2020), but molecular composition or degradability of this carbon pool is largely unknown.

In this study, we collected samples along a spatial transect (~12 km) that followed flow paths of POC released from two mega RTS features (FM3, headwall height up to 10 m, and FM2, approximate headwall height of 25 m; Kokelj et al., 2015). The transect begins at the RTS feature FM3 in the Dempster Creek (tributary of the Stony Creek) and continues to the Stony Creek with additional sampling points in the Stony Creek outlet and in the Peel River (**Figure 2**). Though the Peel River sampling point (P1) is slightly upstream of the Stony Creek outlet, it still integrates slumping signals from Peel Plateau watersheds south of the Stony Creek watershed (e.g., the Vittrekwá watershed). The catchment upstream of RTS feature FM3 drains tall shrub tundra, and then largely forested terrain (especially in the valleys) downstream of FM3 (O'Neill et al., 2015). Catchments upstream of sampling sites T11 and T12 drain mainly tundra. Two stabilized, inactive



RTS features, FM4 and an unnamed thaw slump, here termed “Stabilized thaw slump” (Figure 2), are located along the transect (Malone et al., 2013). While they are stabilized, erosion of their vegetated debris tongues may still deliver thawed permafrost material into the stream, similar to debris tongues of FM2 and FM3. Furthermore, several unimpacted streams join the transect. See **Supplementary Table 1** for exact coordinates of the sampling locations.

Sampling

All samples were collected in July–August 2017. Water samples (around 1 L per location) were collected at each transect point (Figure 2, T1–T12, starting at the outflow of RTS feature FM3), and filtered within 24–48 h through pre-combusted glass-fiber filters (GF/F, Whatman, pore size 0.7 μm) for DOC and POC analyses (bulk elemental and lipid biomarkers) and polyethersulfone membrane filters (PES, Pall Corporation, pore size 0.45 μm) for mineral-specific surface area and py-GCMS analyses. We also collected samples for stable water isotopes ($\delta^{18}\text{O}$ and $\delta^2\text{H}$) which were filtered and stored cool (+5°C) without headspace. All filters (POC samples) were

kept frozen and filtrates (DOC samples) were acidified to pH 2 with high purity 37% HCl, and kept at +5°C in the dark. To understand source materials for the transect, we collected Holocene permafrost and active layer samples from the headwall of FM3, newly thawed debris beneath the slump headwall (headwall debris) from RTS feature FM3, and sediments and suspended particulate matter (SPM) from the outflow and scar zone of RTS features FM3 and FM2 (Figure 2). The SPM from the FM3 scar zone was collected from a mud pool, while for FM2 it was sampled from the rill channels crossing the scar zone. The headwall (active layer, Holocene permafrost and headwall debris) sediment samples from FM3 and sediment samples B1 and T1 are previously reported in Bröder et al. (2021). Fresh sediment deposits were collected with a stainless-steel spoon from stream/river banks at transect locations and scar zones, and were frozen shortly after their collection. The scar zone sediments are likely recently deposited, whereas the sediments collected from the streambanks may be older, yet we collected these samples as close to the stream as possible to ensure them to be recently transported.

Stable Water Isotopes

We measured stable isotopes of oxygen and hydrogen in water ($\delta^{18}\text{O}$ and $\delta^2\text{H}$) along the transect to characterize hydrologic inputs and associated hydrochemical effects from tributary streams. The samples were analyzed with a Picarro Inc L2140-i Wavelength-scanning cavity ring-down spectrometer. Three in-house standards were run before and after a sequence of 10 samples. All the in-house standards were calibrated against international standards VSLAP and VSMOW (from IAEA). The fourth in-house standard, KONA (calibrated against VSLAP and VSMOW), was used to control the precision and accuracy of the measurements ($\text{SD} < 0.1\text{‰}$ for $\delta^{18}\text{O}$ and $< 2\text{‰}$ for $\delta^2\text{H}$). The samples were run in replicates of seven, of which the first three were discarded. The isotope analysis was carried out at the Stable Isotope Laboratory of the Department of Earth Sciences at the Vrije Universiteit Amsterdam, Netherlands.

Mineral-Specific Surface Area Analysis

For mineral-specific surface area (SA) analysis, 0.7–1.0 g of sediment or SPM were subsampled, combusted (at 350°C for 12 h) to remove all organic material and, directly prior to analysis, degassed with N_2 in a vacuum while heated to 300°C for 3 h. The pre-processed samples were analyzed on a Nova 4200e Surface Area Analyzer with Quantachrome software using 5-point BET measurements. The reference material BAM-PM-102 ($5.41 \pm 0.04 \text{ m}^2 \text{ g}^{-1}$) and Quantachrome Instruments Surface Area Reference Material for multi-point BET ($27.46 \pm 3.6 \text{ m}^2 \text{ g}^{-1}$) were used to monitor the instrument performance. All surface area data are reported as $\text{m}^2 \text{ g}^{-1}$. The SA analysis was carried out at the Organic Matter Laboratory of the Department of Earth Sciences at the Vrije Universiteit Amsterdam, Netherlands.

Grain Size Analysis

About 1 g of freeze-dried sediment was subsampled and treated with 5 ml of H_2O_2 together with distilled water to remove all fine organic matter. An additional 5 ml of H_2O_2 was added until complete oxidation, and the sample was boiled. To remove larger organic particles, each sample was filtered and treated again with 5 ml of H_2O_2 and boiled to remove excess water from the filtration process. To remove all calcium carbonates (CaCO_3) the samples were treated with 5 ml of HCl and boiled with 100 ml of water, after which 800 ml of water was added and the sample was let to settle overnight. To break all the charged bonds between clay particles, sodium phosphate ($\text{Na}_4\text{P}_2\text{O}_7 \cdot 10\text{H}_2\text{O}$) was added to each sample with distilled water and boiled. The pre-treated samples were filtered (pore size 1 mm) and analyzed on a Helos/KR laser diffraction particle size and particle size distribution analyzer (Sympatec, GmbH) with a Quixel dispersing system (Sympatec, GmbH) at the Sediment Laboratory of the Department of Earth Sciences at the Vrije Universiteit Amsterdam, Netherlands. All the grain size data are reported as median grain size (μm) or as percentages of different grain size classes. The grain size classes are clay ($< 8 \mu\text{m}$), silt ($8\text{--}63 \mu\text{m}$), and sand ($63\text{--}1000 \mu\text{m}$).

Total Suspended Solids, Bulk Organic Carbon and Carbon Isotope ($\delta^{13}\text{C}$, $\Delta^{14}\text{C}$) Analyses

Prior to analyses, all the sediment and SPM samples were freeze-dried. Pre-weighed GF/F were used for bulk organic matter parameters (POC, TN, $\delta^{13}\text{C}$, and $\Delta^{14}\text{C}$), and to derive total suspended solids (TSS). The concentration of TSS (mg L^{-1}) was calculated by the difference in filter weight before and after filtration which was divided by the volume of water filtered (L).

For the analyses of bulk parameters, total organic carbon content (TOC), stable carbon isotopes ($\delta^{13}\text{C}$) and total nitrogen (TN), sediments were homogenized and subsamples (10–20 mg) were placed into silver capsules. The filters were subsampled by punching approximately 18% of the filter area and put into silver capsules/boats. Both sediment and filter samples were treated by fumigation over concentrated, high purity HCl (37%, 60°C , and 72 h) to remove all inorganic carbon. After fumigation, samples were heated in the presence of NaOH pellets (60°C and a minimum of 48 h) to neutralize any excess acid. The samples were subsequently wrapped in tin capsules. Sediments were sent to the National Research Council, Institute of Polar Sciences in Bologna, Italy and filters to the Stable Isotope Facility (SIF) of the University of California Davis, United States. At the SIF facility, the filters were analyzed for TOC, $\delta^{13}\text{C}$ and TN with an Elementar Vario EL Cube or Micro Cube elemental analyzer (Elementar Analysensysteme GmbH, Hanau, Germany) interfaced to PDZ Europa 20-20 isotope ratio mass spectrometer (Sercon Ltd., Cheshire, United Kingdom) or Isoprime VisION IRMS (Elementar UK Ltd., Cheadle, United Kingdom). In Bologna, the sediment samples were analyzed using a Thermo Fisher Elemental Analyzer (FLASH 2000 CHNS/O) coupled with a Thermo Finnigan Delta plus isotope ratio mass spectrometer (IRMS) for TOC (wt.%), TN (wt.%) and $\delta^{13}\text{C}$. The VPDB (Vienna Pee Dee Belemnite) was used as a reference standard for $\delta^{13}\text{C}$.

The DOC samples were analyzed for carbon concentration and $\delta^{13}\text{C}$ at the Institute for Biodiversity and Ecosystem Dynamics, University of Amsterdam, Netherlands. The samples were measured with an ISO-TOC cube (Elementar GmbH, Langensfeld, Germany) and Isoprime100 (Elementar UK Ltd., Manchester, United Kingdom) repeatedly (five times) of which the first two were discarded to avoid carry-over effects from previous samples. Blanks (ultrapure deionized water acidified to pH 1.9 with 37% HCl) and standards (caffeine $\geq 99\%$ anhydrous, Sigma Aldrich) were run at the beginning and end of each sample sequence. The VPDB was used as an international reference standard for $\delta^{13}\text{C}$ along with IAEA-600, caffeine (^{13}C) and IAEA-CH6, sucrose (^{13}C). Standard deviation of the DOC measurements was 0.2 mg L^{-1} and for $\delta^{13}\text{C}$ 0.2‰ .

For radiocarbon (^{14}C) analysis, filters and sediments (25–35 mg) were subsampled and acid-fumigated as described above. Measurements were performed using a coupled elemental analyzer-accelerator mass spectrometer (EA-AMS) system; the EA used was a vario MICRO cube (Elementar) and the AMS a Mini Carbon Dating System MICADAS (Ionplus, Dietikon, Switzerland) (Synal et al., 2007). The filter samples were blank corrected for constant contamination using a MATLAB code

described in Haghypour et al. (2019). Blank filters were spiked with “radiocarbon dead” and modern reference material in order to monitor and correct for potential contamination during sample processing. For the sediment samples and blank-corrected filters measurement uncertainty is reported in percentages. The analyses were carried out at the Laboratory of Ion Beam Physics at the Swiss Federal Institute of Technology (ETH) in Zürich, Switzerland.

Pyrolysis-Gas Chromatography-Mass Spectrometry (py-GCMS)

For macromolecular analyses, samples were analyzed with a py-GCMS. Solvent-extracted and non-extracted subsamples (10–15 mg) of sediment/SPM were placed into a clean fire-polished quartz tube and pyrolyzed at 700°C for 15 to 20 s in a helium flow. The resulting material was transferred via a heated transfer line to an Agilent 7980A GC fitted with an Agilent HP-5 column coupled to an Agilent 5975 MSD single quadrupole mass spectrometer operated in electron ionization (EI) mode with a scanning range of m/z 50 to 650 at 2.7 scans s^{-1} and ionization energy of 70 eV. The pyrolysis transfer line and rotor oven temperatures were set at 325°C, the heated GC interface at 280°C, the EI source at 230°C and the MS quadrupole at 150°C. Helium was used as the carrier gas, and the samples were introduced in split mode with a split ratio of 20:1 (or 10:1 for samples containing less organic material) and a constant flow of 20 mL min^{-1} . The GC oven was programmed from 40°C (held for 5 min) to 250°C at 4°C min^{-1} , then gradually (20°C min^{-1}) heated to 300°C and held at this temperature for one minute. Blanks (empty quartz tubes) were run after every sample to avoid any material carrying over to the following samples. The analysis was carried out at the Department of Earth and Environmental Sciences at the University of Manchester, United Kingdom.

The acquired ion chromatograms were integrated with MSD Chemstation Data Analysis software (Agilent 2008, version G1701EA E.02.00). Compounds were identified by comparison of relative retention times and spectra to those reported in the NIST library. Given the complexity of the GCMS chromatograms, it was not possible to integrate individual compounds in total ion current mode due to significant overlap between ion peaks. A similar approach, using single ion filtering, was adopted as described in Sparkes et al. (2016). The five compound groups targeted were aromatics (toluene, ethylbenzene, and naphthalene), polysaccharides (3-furaldehyde, furfural, and 5-methylfurfural), lignin markers (guaiacol, creosol, and 4-ethylguaiacol), phenols (phenol, 2-methylphenol, 3-methylphenol, and 4-methylphenol), N-containing compounds (pyridine, 2-methylpyridine, and benzonitrile) and alkanes (carbon chain lengths C9–14). The results are given as relative amounts of the compound group to all identified compound groups in each sample, not as absolute amounts.

Biomarkers: *n*-Alkanes and *n*-Alkanoic Acids

High molecular weight *n*-alkanes (carbon chain lengths C27–33, HMW_{C27–33}) and *n*-alkanoic acids (carbon chain lengths

C24–32, HMW_{C24–32}), originating from the wax layer of leaves, are common biomarkers for terrestrial vascular plants (Eglinton and Hamilton, 1967a,b). We used these biomarkers to assess degradation of organic matter (e.g., van Dongen et al., 2008; Bröder et al., 2016a). The common degradation proxies are HMW acid-to-alkane ratio and carbon preference indices, CPI (see the CPI formula in the **Supplementary Material**), the latter being a ratio of odd to even-numbered *n*-alkanes and even to odd-numbered *n*-alkanoic acids, respectively (Bray and Evans, 1961). High HMW acid-to-alkane ratios and high CPI values generally indicate fresh, less degraded material and low ratios point toward further degradation and maturity. Index values, however, vary among different vegetation types (Eglinton and Hamilton, 1967b). Additionally, we used the ratio of even low molecular weight (LMW) *n*-alkanes (C16, C18, and C20) and odd HMW *n*-alkanes (C27, C29, and C30) as a proxy for microbial degradation (Grimalt and Albaigés, 1987). High even-LMW-to-odd-HMW *n*-alkane ratios indicate high microbial degradation.

Lipid biomarkers (*n*-alkanes and *n*-alkanoic acids) were extracted with a microwave-assisted extraction method as described in Freymond et al. (2017). The freeze-dried sediments (~3 g) and GF/F filters were extracted twice using DCM-MeOH (9:1, v:v) with a MARS 6 (CEM GmbH, Kamp-Lintfort, Germany) microwave at 100°C for 15 min with a 5 min heating ramp. The extracts were saponified by adding 10 ml of KOH in MeOH and heated at 70°C for 2 h. After adding 5 ml of MilliQ water with NaCl, a neutral fraction was separated by back-extracting with hexane. The remaining extracts were acidified to pH 2 with HCl (37%), and acid fractions were separated by back-extracting with hexane-DCM (4:1, v:v). The neutral fractions were further separated into apolar and polar fractions with column-chromatography (5% deactivated SiO₂ column) using hexane-DCM (9:1, v:v) for apolar (*n*-alkanes) and DCM-MeOH for polar (glycerol dialkyl glycerol tetraethers, GDGTs) fractions (GDGTs are not reported in this study). The acid fractions were treated with 1 ml of BF₃-MeOH, heated on a hot plate for 30 min at 80°C to convert acids to their corresponding methyl esters, and subsequently back-extracted with DCM. For a part of the samples, the acid fractions were additionally cleaned over a SiO₂ column (5% deactivated with NaSO₄ on top) by eluting first with hexane, followed by hexane-DCM (4:1, v:v) and DCM. The hexane-DCM fraction was collected for further analysis. The apolar and acid fractions were analyzed using gas chromatography-mass spectrometry (GCMS; Agilent) at the National Research Council, Institute of Polar Sciences in Bologna, Italy, with a capillary column DB-5 (30 m × 250 μm × 0.25 μm; SGE) at an initial temperature of 60°C followed by a ramp of 4°C min^{-1} to the maximum temperature of 300°C, and held at this temperature for 15 min. Commercially available standards (C8–C40 *n*-alkanes and even chain-lengths between C22 and C30 FAMES, Sigma Aldrich) were analyzed daily before running samples. The compounds were identified by comparing retention times and mass spectra of reference standards. The obtained ion chromatograms were integrated using MSD Chemstation Data Analysis software (Agilent 2008, version G1701EA E.02.00). Blanks were run

with each extraction batch, and they were subtracted from the sample concentrations. The concentrations were normalized to the mineral-specific surface area or OC content, and are reported as $\mu\text{g m}^{-2}$ or as $\mu\text{g g}^{-1}$ OC.

RESULTS

In this study, the term “within slump” refers to the following components of the RTS feature: headwall (active layer, Holocene permafrost and headwall debris), scar zone sediments and scar zone (i.e., rill water or mud pool) particulate organic matter. Sediments within thaw slump component for multiple RTS features on the Peel Plateau are described in Bröder et al. (2021), while the focus of this study is on suspended particulate matter.

Stable Water Isotopes

The outflow from RTS feature FM3 (beginning of the transect) was characterized by a relatively depleted water isotope ($\delta^{18}\text{O}$) signal, ranging from -24 to -25.5‰ (Figure 3A). These values were comparable to the Holocene permafrost pore water/ground ice value of -24.8‰ , previously reported by Bröder et al. (2021). On the scar zone, $\delta^{18}\text{O}$ signal was -21.8‰ in a mud pool, while in the unimpacted streams the values were around -20‰ (Supplementary Table 2). From T7 onward (where water is received from the broader Stony Creek catchment), the $\delta^{18}\text{O}$ signal stayed relatively stable around -20.0‰ .

Total Suspended Solids, Mineral-Specific Surface Area, and Grain Size

The RTS features FM3 and FM2 (inflow to the transect) both released several orders of magnitude higher amounts of TSS than unimpacted streams (Figure 3A; see also Kokelj et al., 2013; Shakil et al., 2020). For RTS feature FM3, TSS was about $32,000 \text{ mg L}^{-1}$ at the outflow from the thaw slump (at T1) and for RTS feature FM2 it was as high as $492,900 \text{ mg L}^{-1}$ (at B1), while in unimpacted streams (N1 and N2) TSS ranged from 29 to 41 mg L^{-1} (Supplementary Table 2). Concentrations of TSS gradually declined downstream: by the time the stream reaches Stony Creek ($\sim 12 \text{ km}$ downstream) TSS was around 900 mg L^{-1} .

Mineral-specific surface area (SA, $\text{m}^2 \text{ g}^{-1}$) along the transect was consistently higher for SPM than for the streambank sediments (Figure 3B). Both for SPM and sediments, SA showed a decreasing trend from higher SA (about $40 \text{ m}^2 \text{ g}^{-1}$ and $25 \text{ m}^2 \text{ g}^{-1}$, respectively) at T1 to lower SA (about $20 \text{ m}^2 \text{ g}^{-1}$ and about $10 \text{ m}^2 \text{ g}^{-1}$, respectively) with increasing distance. Grain size data showed that RTS feature FM2 delivers coarser material (median grain size $\sim 11 \mu\text{m}$ at B1) than RTS feature FM3 ($\sim 6 \mu\text{m}$ at T1). This is seen in the dominance of clay (54%) over silt and sand (39% and 7%, respectively) in the outflow from FM3 (at T1), while after inflow from FM2 (at T7), silt (55%) was the dominant fraction with slightly higher contribution of sand (24%) over clay (22%). Grain size distributions for sediments support the surface area patterns: lower median grain size in the first two

kilometers of the transect compared to higher median grain size downstream (Figure 3B).

Organic Carbon and Total Nitrogen Concentrations and Organic Carbon Loadings

Total organic carbon (TOC,%) of RTS feature FM3 active layer varied from 4.0 to 9.2%, while Holocene permafrost and headwall debris OC content was significantly lower with 1.3 and 1.5%, respectively (Supplementary Table 3). Within the scar zone of FM3, sediment TOC ranged from 1.8 to 2.3%, and for POC it was 4.0%. Total nitrogen (TN) followed a similar pattern as TOC, showing highest values for active layer (0.4–0.6%), followed by headwall debris and Holocene permafrost (both 0.1%) and scar zone sediments (0.1–0.2%). For scar zone SPM, TN was 0.3%. Molar total organic carbon to total nitrogen ratios (TOC:TN) for active layer varied between 11.4 and 14.5, while for permafrost it was 10.0, and for headwall debris 11.1 (Supplementary Table 3). Scar zone sediments and SPM ranged between 12.1 and 13.9. See Supplementary Tables 3, 4 for complete TOC, TN and TOC:TN data.

The RTS features FM2 and FM3 released high amounts of POC (Figure 4A) with concentrations orders of magnitude greater than in unimpacted streams, which were all below 2.0 mg L^{-1} . The POC concentrations in the outflow from FM3 were highest, around 600 mg L^{-1} , gradually declining to $<100 \text{ mg L}^{-1}$ within two kilometers. Along the transect, POC content varied between 1.8 and 3.4%. The TN concentrations followed the POC pattern with highest concentrations at the FM3 outflow (54.3 mg L^{-1}) which then declined to $<1 \text{ mg L}^{-1}$ at T6. Along the transect, TN varied between 0.1 and 0.3% with the highest values at T5 (0.2%) and T6 (0.3%). The TOC:TN ratio increased gradually from 10.5 at T1 to 15.5 at the outflow from FM2 (at T7) with a drop to 11.2 at T6 (Supplementary Table 4). Along the rest of the transect, the TOC:TN ratio remained at ~ 14 . See Supplementary Table 4 for POC, TN and TOC:TN data.

Concentrations of DOC were an order of magnitude lower than those of POC, ranging between 5.0 and 14 mg L^{-1} throughout the transect with no apparent trends (Figure 4A and Supplementary Table 4). The unimpacted streams had higher DOC concentrations ($\sim 14 \text{ mg L}^{-1}$) than the outflow from RTS features FM2 and FM3 ($6\text{--}8 \text{ mg L}^{-1}$).

The TOC contents for streambank sediments along the transect varied between 0.6 and 1.4% (Figure 4B). The first three kilometers of the transect had higher TOC than farther downstream (about 1.4% and 0.8% on average, respectively). The TN varied between 0.09 and 0.13% with a decreasing trend downstream (until T8). The molar TOC:TN ratios showed an increasing trend downstream, from 11.1 at T1 to 14.3 at T11 (Supplementary Table 3).

Mineral-specific surface area-normalized organic carbon loadings (mg m^{-2}) for SPM and streambank sediments varied between 0.5 and 1 mg m^{-2} with an increasing trend downstream (Figure 4C). At T8, stream inflow increased OC loading of SPM to $\sim 1 \text{ mg m}^{-2}$, whereas sediment OC loading decreased to $\sim 0.5 \text{ mg m}^{-2}$.

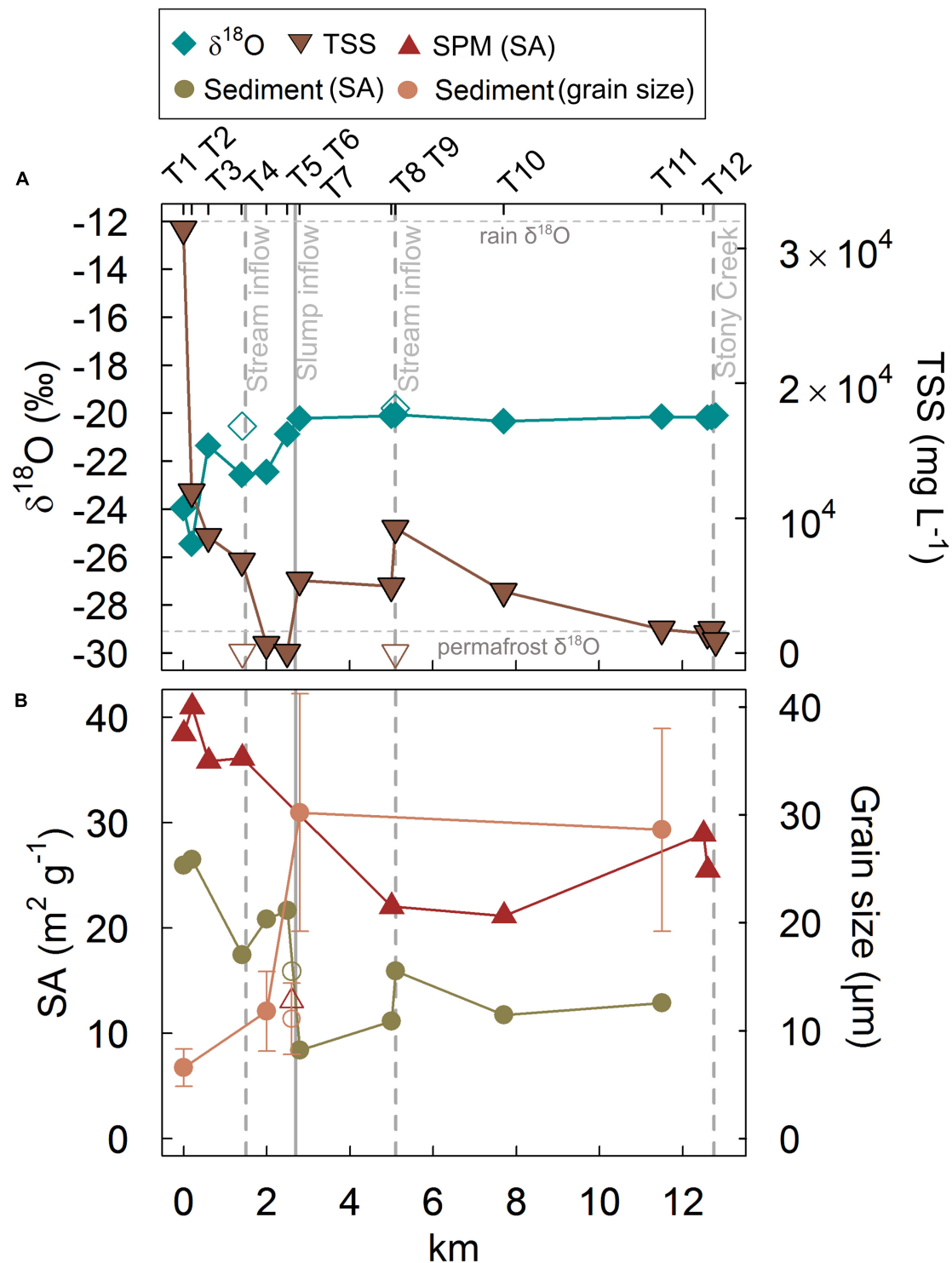
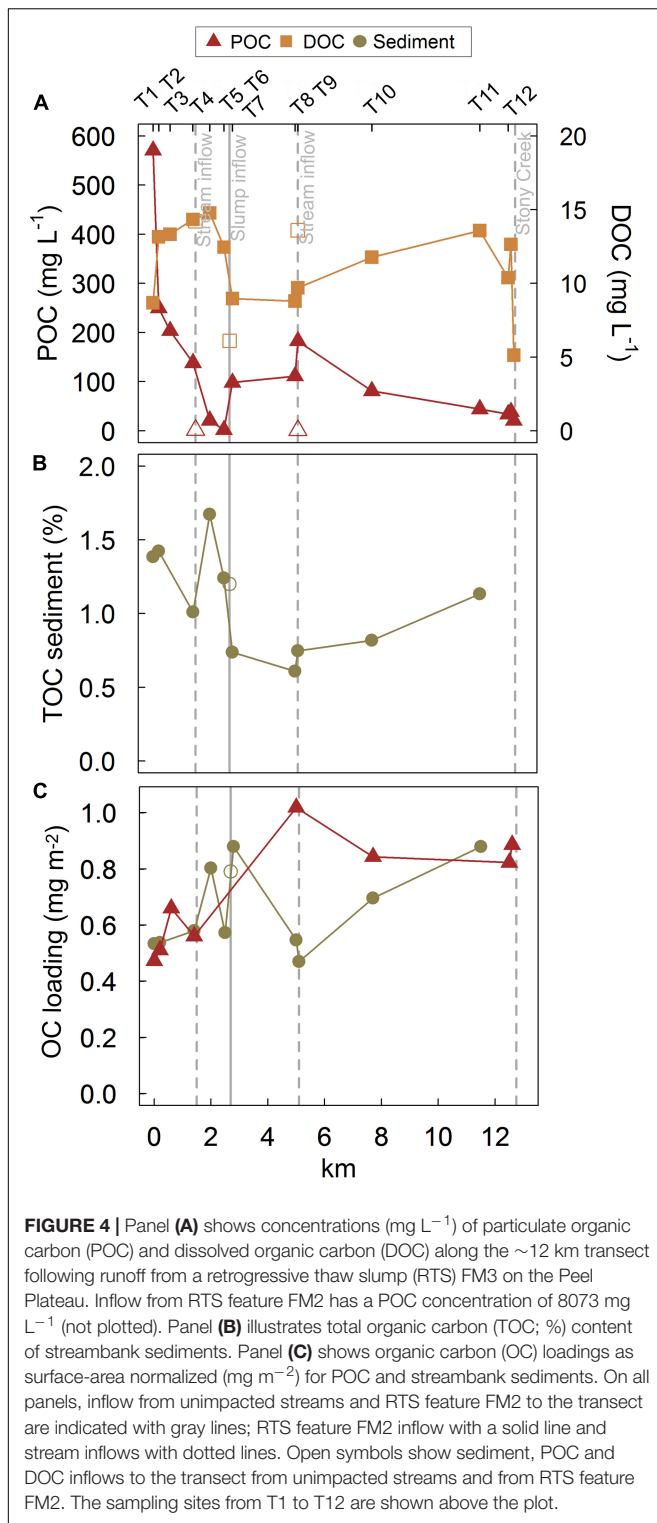


FIGURE 3 | (A) Water (oxygen) isotope $\delta^{18}\text{O}$ (‰) and total suspended solids (TSS; mg L^{-1}) along the ~12 km transect following runoff from a retrogressive thaw slump (RTS) FM3 on the Peel Plateau. The TSS for inflow from RTS feature FM2 (sampling point B1 in **Figure 2**) is too high ($49 \times 10^5 \text{ mg L}^{-1}$) to plot on the figure. **(B)** Mineral-specific surface area (SA; $\text{m}^2 \text{g}^{-1}$) of suspended particulate matter (SPM) and streambank sediments along the transect. The sediment median grain size (μm) with standard deviation is also shown. The vertical gray lines indicate RTS feature FM2 inflow (solid line) and stream inflows (dotted lines). The horizontal gray lines indicate $\delta^{18}\text{O}$ of rain (-12.0‰) and Pleistocene permafrost (-29.1‰) (Zolkos and Tank, 2019). Open symbols show inflows to the transect from unimpacted streams and/or RTS feature FM2. The sampling sites from T1 to T12, as given in **Figure 2** are shown above the plot.



Carbon Isotopes ($\delta^{13}\text{C}$, $\Delta^{14}\text{C}$)

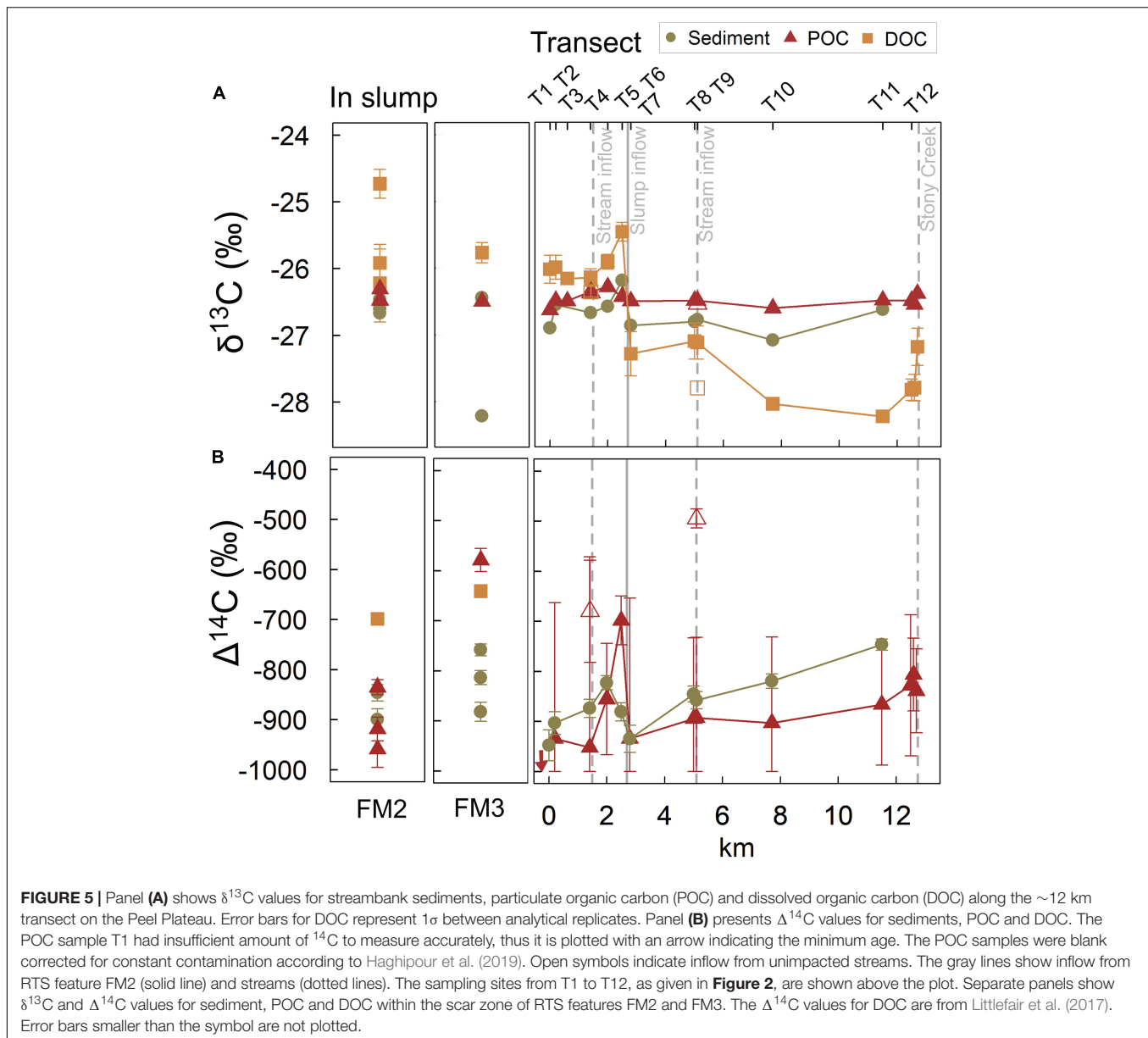
Within RTS feature FM3, the $\delta^{13}\text{C}$ for DOC was less depleted (-25.8‰) than POC (-26.5‰) or the scar zone sediments (from -28.2 to -26.4‰). Within FM2, the $\delta^{13}\text{C}$ for DOC varied between -26.2 and -24.7‰ , POC from -26.5 to -26.3‰ and

scar zone sediments from -26.7 to -26.5‰ (Figure 5A). The $\delta^{13}\text{C}$ for POC and streambank sediments remained relatively stable throughout the whole transect (Figure 5A) with the $\delta^{13}\text{C}$ -POC ranging between -26.3 and -26.6‰ , and $\delta^{13}\text{C}$ for streambank sediments from -26.2 to -27.1‰ . The $\delta^{13}\text{C}$ -DOC showed more variability with values between -25.5 and -28.0‰ . The $\delta^{13}\text{C}$ values for streambank sediment OC and DOC decreased by 0.5‰ and 2.0‰ , respectively, after the inflow from RTS feature FM2 (at T7). See Supplementary Tables 3, 4 for complete $\delta^{13}\text{C}$ data.

The $\Delta^{14}\text{C}$ values within the scar zone of FM3 were -579‰ (uncalibrated ^{14}C age of 6,900 years) for POC and varied from -758 to -885‰ (11,400–17,000 years) in the sediments (Figure 5B). Within the scar zone of RTS feature FM2, the $\Delta^{14}\text{C}$ values were slightly lower, ranging from -835 to -959‰ for POC and from -846 to -994‰ for sediments, corresponding to ^{14}C ages between 14,400 and 25,600 years for POC and 15,000 and 40,600 years for sediments, respectively. Similarly, for both streambank sediment OC and POC, $\Delta^{14}\text{C}$ values were low, varying between -700 and -900‰ (10,000 and 25,000 years), although sediment OC was generally more ^{14}C -enriched (younger) than POC (Figure 5B). Both POC and sediment showed a trend of increasing $\Delta^{14}\text{C}$ values (i.e., from older to younger ^{14}C ages) along the transect. Streambank sediments and POC in the outflow from RTS feature FM3 (at T1) were older, $<-940\text{‰}$ ($>23,000$ ^{14}C years old) than those from the outflow of FM2 (at B1) with -860‰ ($\sim 14,600$ ^{14}C years old). POC in the unimpacted streams was younger, between -500 and -680‰ (5,000–10,000 ^{14}C years old), than in the RTS feature outflow (Figure 6). See Supplementary Table 5 for the complete radiocarbon data.

(Macro)molecular Composition of SPM and Streambank Sediments

We used py-GCMS data to track relative changes in the macromolecular composition of SPM and sediments. Polysaccharides and lignin moieties are considered fresh and easily degradable, whereas aromatics and (short-chained) alkanes are thought to be more recalcitrant (Guo et al., 2003; Sparkes et al., 2016). N-containing compounds have been shown to indicate microbial activity (Vancampenhout et al., 2009). Our analyses indicate that sediments within RTS feature FM3 (Holocene permafrost, headwall debris and scar zone) consist primarily of aromatics, phenols and alkanes with contributions 63–80%, 17–21%, and 6–12%, respectively, and only minor contribution of polysaccharides 0–2% (Figure 7). The active layer of FM3 showed a slightly different distribution pattern with relatively high contribution of polysaccharides (35 to 43%) and a minor contribution of lignin compounds (1 to 6%). Along the transect, aromatic moieties dominated in all SPM and streambank sediment samples with contributions varying between 51 and 87% (Figure 7). The macromolecular composition of the SPM samples was further characterized by the presence of substantial amounts of phenols from 10 to 29%, alkanes 4–14%, N-containing compounds 2–13% and minor amounts of polysaccharides 0–2%. Other than aromatics,

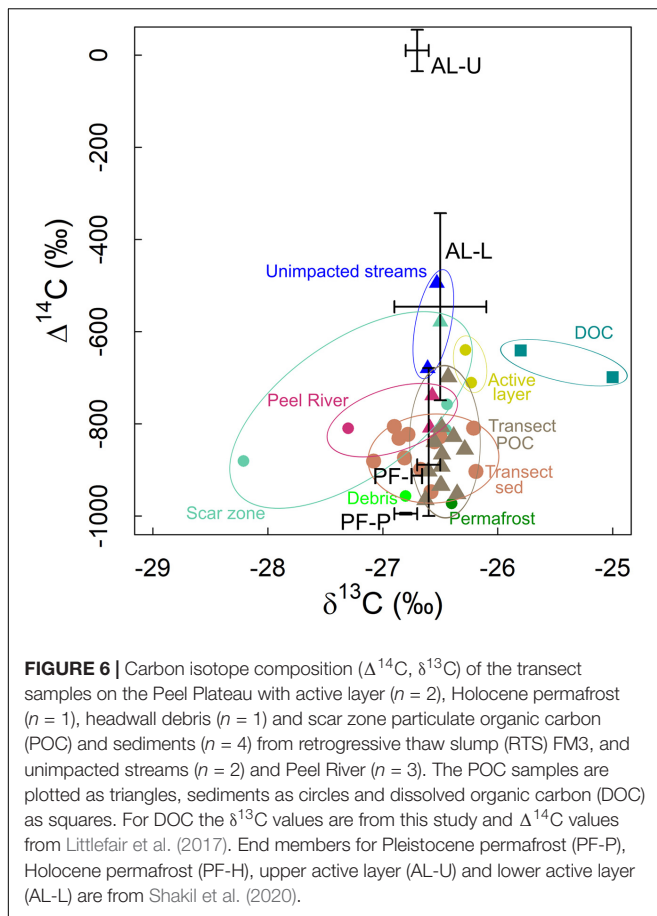


streambank sediments along the transect contained 0–36% of phenols, 0–11% of N-containing compounds, 7 to 13% of alkanes and <1% of polysaccharides. See **Supplementary Table 6** for complete py-GCMS data.

Lipid biomarker analysis was used to characterize the molecular composition (i.e., vascular plant input) of sediments and POC, and to investigate their degradation status. The sediment samples from the active layer, Holocene permafrost and headwall debris of FM3, and sediment samples at T1 and at B1 are the same samples that Bröder et al. (2021) have reported, but were extracted separately for this study. Lipid biomarker analyses show that concentrations of $\text{HMW}_{\text{C}_{27-33}}$ *n*-alkanes in the active layer varied between 250 and 360 $\mu\text{g g}^{-1}$ OC, in Holocene permafrost the concentration was 94 $\mu\text{g g}^{-1}$ OC and in the scar zone sediments of FM3 ~390 $\mu\text{g g}^{-1}$ OC (**Supplementary**

Table 7). Concentrations of $\text{HMW}_{\text{C}_{24-32}}$ *n*-alkanoic acids in the active layer ranged between 3500 and 5500 $\mu\text{g g}^{-1}$ OC, and are an order of magnitude higher than in Holocene permafrost (630 $\mu\text{g g}^{-1}$ OC) or in the scar zone sediments within FM3 (540–1,340 $\mu\text{g g}^{-1}$ OC). Along the transect, the $\text{HMW}_{\text{C}_{27-33}}$ *n*-alkane concentrations varied between 60 to 346 $\mu\text{g g}^{-1}$ OC for SPM and from 104 to 203 $\mu\text{g g}^{-1}$ OC for streambank sediments (**Supplementary Tables 7, 8**). The $\text{HMW}_{\text{C}_{24-32}}$ *n*-alkanoic acid concentrations ranged from 88 to 1130 $\mu\text{g g}^{-1}$ OC for SPM and from 24 to 461 $\mu\text{g g}^{-1}$ OC for streambank sediments.

Holocene permafrost, headwall debris and scar zone sediments showed loadings (i.e., mineral-specific surface-area normalized concentrations) of $\text{HMW}_{\text{C}_{24-32}}$ *n*-alkanoic acids between 0.25 and 1.96 $\mu\text{g m}^{-2}$ and of $\text{HMW}_{\text{C}_{27-33}}$ alkanes 0.06 and 1.12 $\mu\text{g m}^{-2}$ (**Figure 8**). Only the active layer showed higher



HMW_{C24-32} *n*-alkanoic acid loadings (up to 6.62 $\mu\text{g m}^{-2}$), yet the HMW_{C27-33} *n*-alkane loadings (0.31 to 0.47 $\mu\text{g m}^{-2}$, **Figure 8**) were as low as for Holocene permafrost, headwall debris and scar zone sediments. Throughout the transect, loadings of both HMW *n*-alkanoic acids and *n*-alkanes were in a similar range for SPM and streambank sediments with the exception of *n*-alkanoic acids in SPM at the beginning of the transect (at T2, **Figure 8**). For the streambank sediments, HMW_{C27-33} *n*-alkane and HMW_{C24-32} *n*-alkanoic acid loadings varied from 0.04 to 0.14 $\mu\text{g m}^{-2}$ and 0.01 and 0.41 $\mu\text{g m}^{-2}$, respectively. For SPM, loadings ranged from 0.05 to 0.35 $\mu\text{g m}^{-2}$ and 0.16 and 0.75 $\mu\text{g m}^{-2}$, respectively.

The HMW_{C24-33} acid-to-alkane ratio, used to assess degradation status of organic matter (higher ratio indicates fresher organic matter), showed the highest ratio for the active layer (~ 15) followed by Holocene permafrost (~ 7) and headwall debris and scar zone sediments (~ 3). Along the transect, acid-to-alkane ratios ranged between <1 and 7 for SPM and between <1 and 4 for streambank sediments (**Figure 9A**). The CPI values (another degradation proxy, with higher CPI indicating fresher material) for *n*-alkanoic acids ranged between 5 and 6 within RTS feature FM3 (active layer, Holocene permafrost, headwall debris and scar zone sediments) while CPI values for *n*-alkanes varied between 4 and 8, with the highest values for Holocene permafrost and active layer (**Figure 9B**). Along the transect, CPI values for

n-alkanes ranged between 3.6 and 8.5 for SPM and between 1.8 and 6.8 for streambank sediments (**Figure 9B**). For *n*-alkanoic acids, CPI values varied from 3.6 to 5.8 for SPM and from 3 to 6 for streambank sediments (**Supplementary Tables 7, 8**).

DISCUSSION

The first part of the discussion is focused on source materials (active layer, Holocene permafrost, headwall debris and scar zone sediments) within RTS feature FM3 (see section “Within the Slump: RTS Features as Sources of Water and Organic Matter”), followed by a discussion on the transport of OC along the transect (see section “Beyond the Thaw Slump: Transport and Degradation Status of Sediments and SPM”) and a final section (“The Role of RTS Features on the Peel Plateau Organic Carbon Dynamics”) on the role of the RTS features on the Peel Plateau organic carbon dynamics.

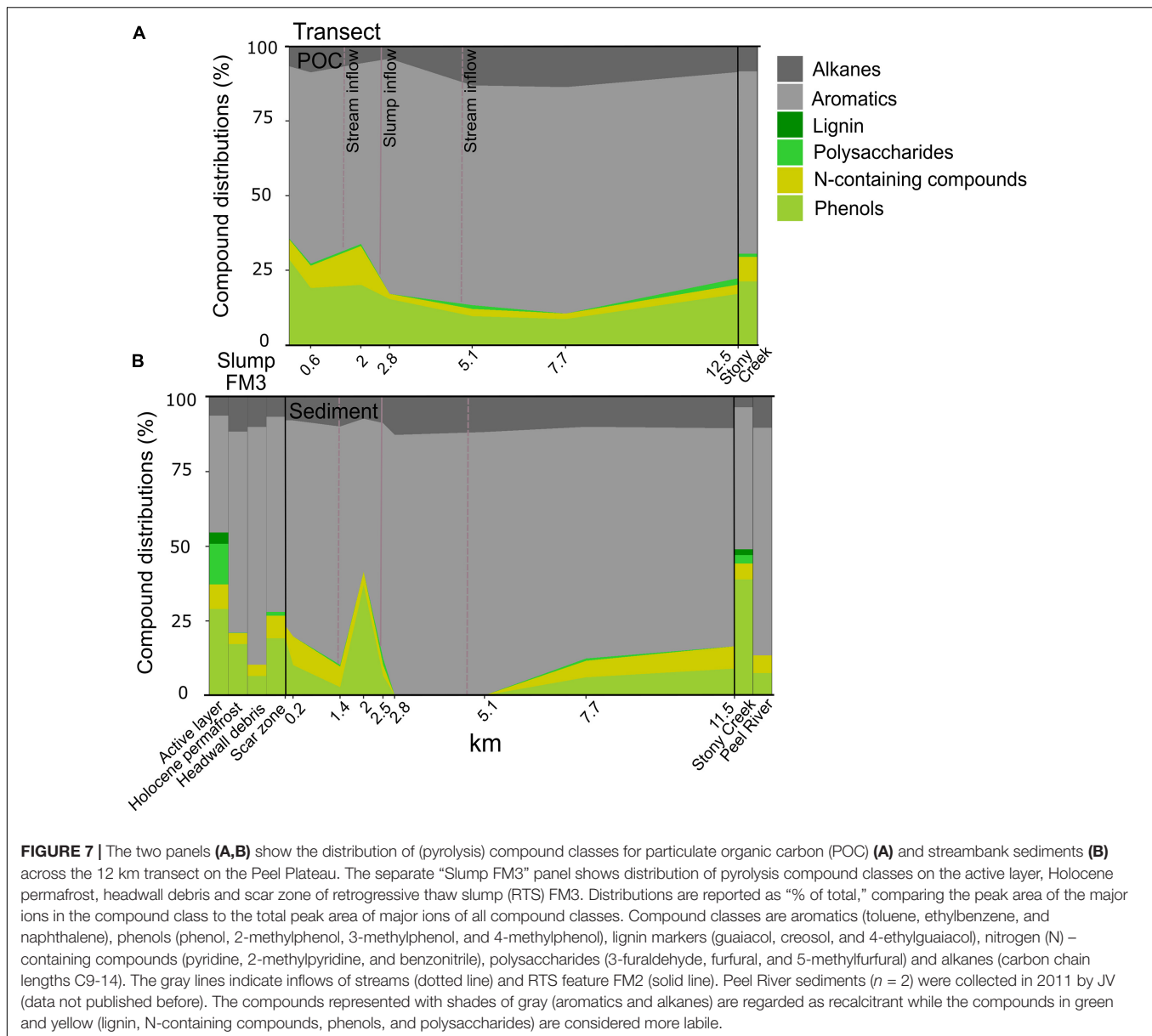
Within the Slump: RTS Features as Sources of Water and Organic Matter

In this section we show that Holocene permafrost is comprised mostly of recalcitrant matter, while the active layer is characterized by more labile matter such as polysaccharides. The scar zone organic matter is defined as a mixture of active layer and permafrost. Our data suggest that some degradation processes may take place immediately upon thaw on the RTS headwall and within the scar zone. These processes are confined largely on the active layer component, as permafrost-derived OC is not as readily degradable.

Bulk Characteristics of the Transect Source Materials

Within the FM3 scar zone, the $\delta^{18}\text{O}$ signature in the mud pool (-21.8‰) likely represents Pleistocene and Holocene permafrost ice meltwater (-29.1‰ and -24.6‰ , respectively, Zolkos and Tank, 2019) mixed with active layer soil waters and/or summer precipitation (-12‰ in Fort McPherson; Zolkos and Tank, 2019) and is subjected to some evaporative enrichment (Jasechko, 2019). The DOC concentration of the scar zone mud pool is higher (18.2 mg L^{-1}) than values reported by Littlefair et al. (2017) for scar zone flowing rillwater ($\sim 10 \text{mg L}^{-1}$). This could be related to longer residence time in pools and evaporative enrichment, as well as to the relatively dry sampling conditions in 2017, limiting dilution of DOC concentrations by rain events that may have been the case in other years. Likely most of the DOC comes from the Holocene permafrost or the active layer as DOC concentrations in Pleistocene permafrost are much lower (Zolkos and Tank, 2019; Shakil et al., 2020). This is supported by the relatively young ^{14}C -DOC ages (from 8,200 to 9,600 years; Littlefair et al., 2017) within the scar zones of FM3 and FM2 (**Figure 5B**).

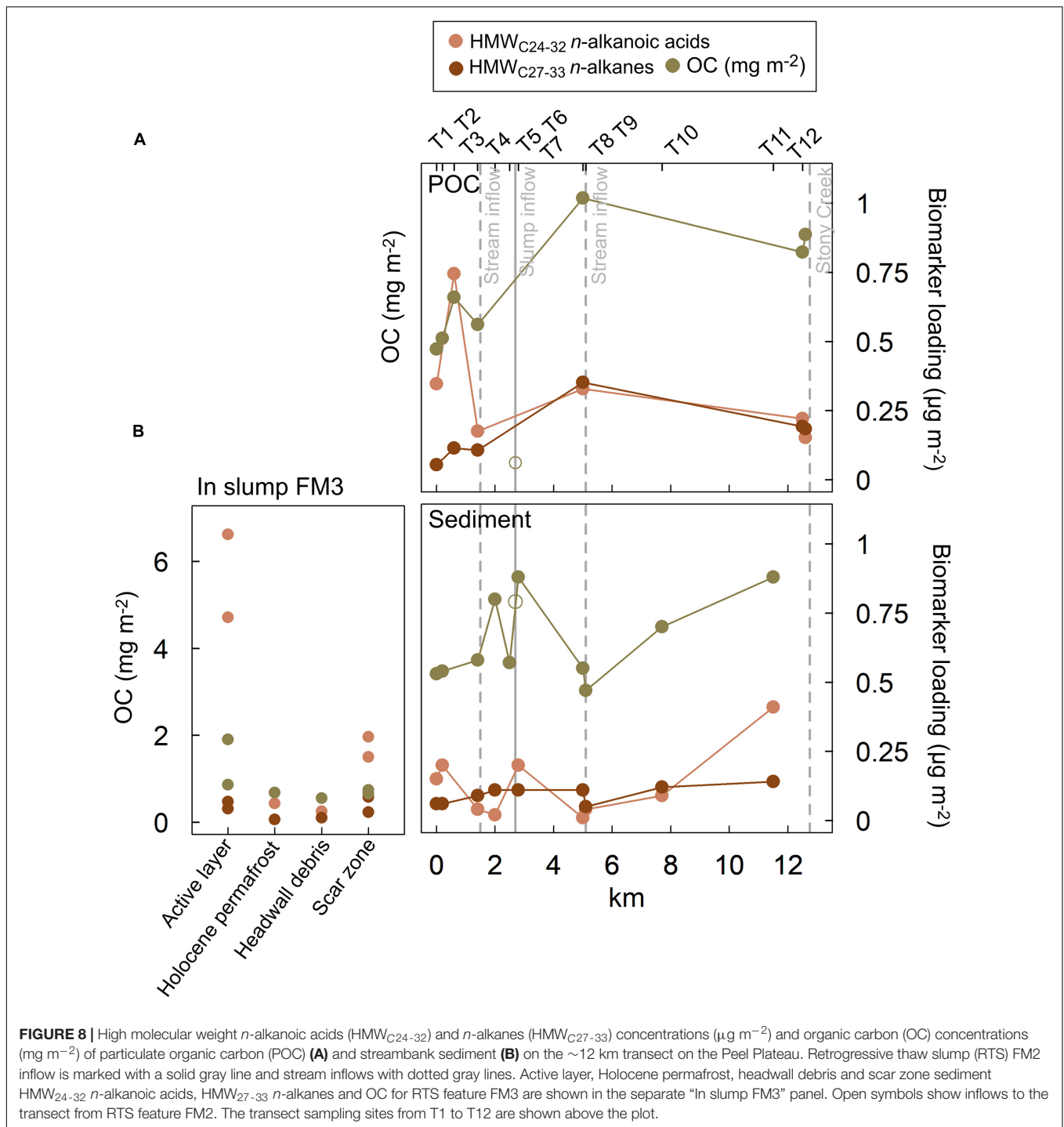
Within FM3, OC content of the scar zone sediments (1.3–1.5%) is similar to the Holocene permafrost and headwall debris (1.4%), suggesting a larger contribution from permafrost than from the active layer ($\sim 4\text{--}9\%$), or degradation of the latter (Bröder et al., 2021). However, SPM (sampled from a mud pool) within the scar zone shows a higher OC content, $\sim 4\%$, suggesting



either a stronger influence of the active layer organic matter, preferential export of finer, relatively OC-rich permafrost, or potentially primary production within the relatively less turbid standing water pools of the scar zone. The molar TOC:TN ratio, which is used to assess sources and degradation of organic matter, is most varied in the active layer (11.4–14.5) followed by scar zone sediments (12.1–13.9), headwall debris (11.1) and Holocene permafrost (10.0) (Supplementary Table 3). Values > 10 indicate a fresh terrestrial origin and values of around 4–10 aquatic production, while degradation of organic matter decreases the ratio (Meyers, 1994; Schmidt et al., 2000). Our TOC:TN ratios are in the similar range as the values reported by Lacelle et al. (2019) in the same region, yet are lower than the ones observed in the deep mineral- and organic soils (C:N > 20) on the Alaskan tundra (Plaza et al., 2019), indicating a potentially higher degree of OC

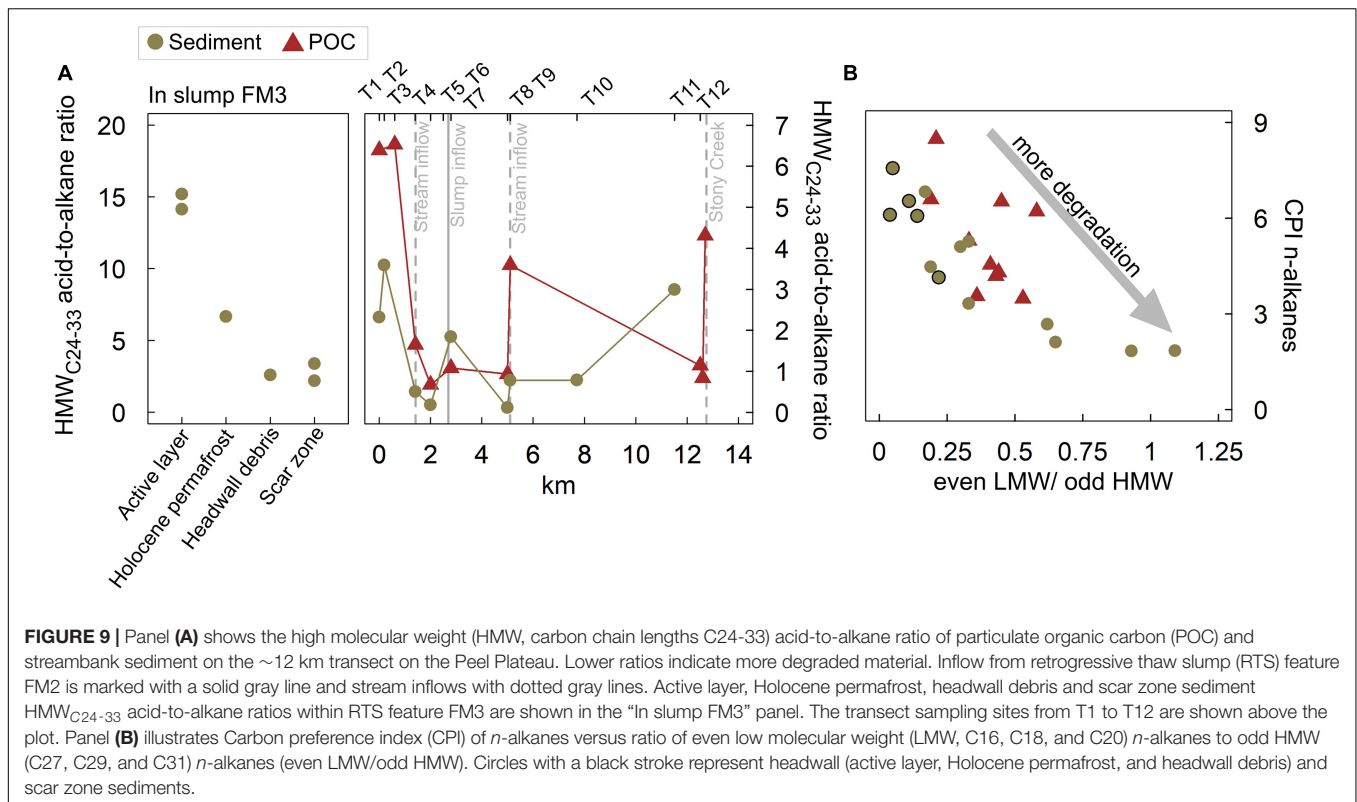
degradation on the Peel Plateau. Lacelle et al. (2019) suggest that OC in the Pleistocene-permafrost may indeed be degraded and that cryoturbation, albeit limited, could explain the low TOC:TN values of the Holocene-layer.

On the Peel Plateau, the $\delta^{13}\text{C}$ signatures of active layer, Holocene- and Pleistocene permafrost overlap (from -28 to -26‰ ; Shakil et al., 2020), but radiocarbon (^{14}C) data show a larger distinction between these sources (Figure 6; see also Shakil et al., 2020). The $\Delta^{14}\text{C}$ of scar zone POC (sampled from a mud pool) is -580‰ (7,000 years), which suggests an additional source of modern carbon. Given the young age and terrestrial $\delta^{13}\text{C}$ signature (-26.5‰) of the POC, it likely derives from the active layer (from -640 to -770‰ , in years from 8,000 to 9,900, respectively) or re-vegetation of the scar zone rather than aquatic sources (mean $\delta^{13}\text{C}$ of $-33.4 \pm 4.2\text{‰}$ and



$\Delta^{14}\text{C}$ of $-145 \pm 145\%$, Shakil et al., 2020). Sediments within FM3 scar zone are older (between -760 and -880% , 11,300–17,000 years old) with $\delta^{13}\text{C}$ values between -26.4 and -28.2% . These differences display the heterogeneity within the scar zones, and the depleted $\delta^{13}\text{C}$ signature may indicate hot spots for autochthonous production (Figure 6). Within FM2, $\Delta^{14}\text{C}$ of the scar zone POC (sampled from rill channels) ranges between -920 and -960% (20,000–25,600 years) while that of sediments

varies between -900 and -990% (18,000 to 40,600 years). These differences within the scar zone POC of FM2 and FM3 may be due to different hydrodynamic settings at sampling locations (i.e., mud pool at FM3 and rill channels at FM2), suggesting that stagnant water pools in the scar zone may be comprised of different POC than the rill channels with flowing water. The POC ages are comparable to outflow from Pleistocene-aged Yedoma deposits in Siberia, but the Peel Plateau DOC is 10,000



to 15,000 years younger than DOC originating from Yedoma (Vonk et al., 2013). This could be due to build-up of DOC in Yedoma over time as concentrations there are much higher than on the Peel Plateau (Vonk et al., 2013; Ewing et al., 2015; Littlefair et al., 2017), likely due to the contrasting origin of these deposits and permafrost history of these regions (Tank et al., 2020). Furthermore, the geological history of these two regions differs as the Peel Plateau was glaciated during the Last Glacial period (ca. 18,500-15,000 yr BP, Zazula et al., 2009; Lacelle et al., 2013), thus it is characterized by relatively OC-poor deposits, and hosts glacial tills bearing petrogenic OC from underlying shale bedrock, whereas Yedoma regions remained ice-free and incorporated organic matter from vegetation during aggradation (Yunker et al., 2002; Lacelle et al., 2013; Ewing et al., 2015; Strauss et al., 2017). Petrogenic materials, such as shales, are known to be present in the lower Mackenzie River (Carey et al., 1990; Yunker et al., 2002), and account for 10–30% of the suspended OC load in the Mackenzie Delta (Hilton et al., 2015).

Macromolecular Analyses Suggest a Dominance of Recalcitrant Components in the Scar Zone

The macromolecular composition of organic matter may provide information on the overall lability or recalcitrance of the bulk organic matter, as certain compounds are chemically more prone to degradation than others. High relative contributions of pyrolysis-products of polysaccharides (3-furaldehyde, furfural, 5-methylfurfural) and lignin moieties (i.e., methoxyphenols) indicate organic matter freshness

(Guo et al., 2003), while aromatic products are attributed to more refractory macromolecular precursors and linked to mature OC (Guo et al., 2003; Sparkes et al., 2016), similar to aliphatics (i.e., short-chained alkanes). High relative abundances of N-containing compounds have been shown to indicate a higher degree of microbial activity and decomposition (Vancampenhout et al., 2009). Alkylphenols (e.g., 2-methylphenol and 3-methylphenol) are common pyrolysis moieties of terrestrial material and may originate from various precursor biomacromolecules including polysaccharides and proteins (Van Heemst et al., 1999; Guo et al., 2003, 2009; Xu et al., 2009).

All lignin markers (guaiacol, creosol, and ethylguaiacol) along with the majority of polysaccharide markers are not present within the scar zone sediments, suggesting rapid degradation of these compounds, which are considered amongst the more readily degradable components of soil organic matter, upon thaw (Dai et al., 2002 and references within). Alternatively, the relative decrease of these compounds on the scar zone sediments compared to the active layer may be due to mixing with the permafrost mineral soil. The thawed material (e.g., headwall debris, scar zone sediments) consists largely of recalcitrant compounds. These compositional findings are in line with those of Lacelle et al. (2019) based on ¹³C nuclear magnetic resonance spectroscopy of soils in the Peel Plateau region. The possible dissociation and transfer of polysaccharides or non-mineral bound lignin from particulate to dissolved phase is unlikely, given the orders-of-magnitude lower DOC concentrations compared to mobilized POC (Matiasek and Hernes, 2019).

Lipid Biomarker Data Suggest a Mixture of Biogenic and Petrogenic Organic Matter Within the RTS Feature

Within RTS feature FM3, concentrations of HMW_{C27-33} *n*-alkanes (active layer 250–360 $\mu\text{g g}^{-1}$ OC, Holocene permafrost 94 $\mu\text{g g}^{-1}$ OC and scar zone sediments $\sim 390 \mu\text{g g}^{-1}$ OC) are similar to values reported for coastal and river erosion sites in the Siberian Arctic, where HMW_{C27-33} *n*-alkanes range from 37 to 230 $\mu\text{g g}^{-1}$ OC on a river erosion site (Olenek Channel) and 48–6,355 $\mu\text{g g}^{-1}$ OC on an active coastal erosion site (Muostakh Island) (Sánchez-García et al., 2014; values recalculated to match the carbon chain lengths used in this study). Within RTS feature FM3, the HMW_{C24-32} *n*-alkanoic acid concentrations in the active layer (3,500–5,500 $\mu\text{g g}^{-1}$ OC), Holocene permafrost (630 $\mu\text{g g}^{-1}$ OC) and in the scar zone sediments (540–1,340 $\mu\text{g g}^{-1}$ OC) fall in the lower end of those observed in the Olenek Channel (375 to 50,785 $\mu\text{g g}^{-1}$ OC) and on Muostakh Island (358 to 15,941 $\mu\text{g g}^{-1}$ OC) (Sánchez-García et al., 2014). The higher lipid concentrations in the active layer indicate more vascular plant input and/or less degradation than in the permafrost. The difference in lipid concentrations between the Siberian sites and the Peel Plateau may be due to similar reasons, or as discussed previously, due to differing depositional histories of these landscapes as Yedoma in Siberia hosts OC-rich loess deposits, while the Peel Plateau is characterized by OC-poor glacial tills and glaciofluvial and glaciolacustrine sediments (Schirrmeister et al., 2011; Lacelle et al., 2013).

Active layer samples show the highest HMW acid-to-alkane ratio, implying that they are the least degraded, followed by Holocene permafrost and the scar zone sediments (Figure 9A). The headwall debris of FM3, is more degraded than the active layer or Holocene permafrost, suggesting that some degradation processes may occur immediately upon permafrost thaw. This implies that part of the OC, especially from the active layer, is labile, as has been shown in the ice complex deposit outcrops in Siberia (Sánchez-García et al., 2014). In the scar zone sediments, the HMW-acid-to-alkane ratio is lower than for active layer and Holocene permafrost, suggesting either further degradation processes within the scar zone or mixing with the deeper Pleistocene permafrost. Bacterial activity in the scar zone is likely, given the warm and wet conditions in the scar zone sediments (Cory et al., 2013; van der Sluijs et al., 2018). On Herschel Island (Yukon coast, Canada), it has been shown, using lipid biomarkers, that permafrost organic material released from a coastal RTS degrades before exiting the slump (Tanski et al., 2017).

Within RTS feature FM3, CPI values are similar among active layer, Holocene permafrost and scar zone sediments (from 6 to 8 for *n*-alkanes and from 5 to 6 for *n*-alkanoic acids, see Supplementary Table 7). In the Siberian permafrost outcrops, the CPI values for *n*-alkanes indicate much less degradation with values up to 38 in the Olenek Channel and between 3 and 43 on Muostakh Island (Sánchez-García et al., 2014). The respective *n*-alkanoic acid CPI values are 6 to 13 and 7 to 11 (only Muostakh Slope 7). On the Peel Plateau, the low *n*-alkane CPI values may be explained by the influence of petrogenic carbon sources which usually have CPI values close to one (Bray and Evans, 1961).

Beyond the Thaw Slump: Transport and Degradation Status of Sediments and SPM

In this section we show that the concentrations of POC decrease rapidly in the RTS runoff with distance, while the oldest organic matter is transported kilometers downstream in the POC fraction. Apart from degradation processes in the immediate outflow from the RTS feature, runoff consists largely of recalcitrant compounds that do not seem to degrade during downstream transport. These findings suggest that a large proportion of the organic carbon mobilized from the RTS features on the Peel Plateau is not rapidly degrading during downstream transport, thus the climate impact of the particulate fraction carried by thaw streams is likely relatively small.

Thaw Slump Signal Is Strongest Within the First Few Kilometers of the Runoff

The water isotope data on the transect show that RTS feature FM3 outflow with a $\delta^{18}\text{O}$ value of around -25‰ comprises a mixture of Pleistocene and Holocene permafrost (-29.1‰ and -24.6‰ , respectively, Zolkos and Tank, 2019) and active layer/precipitation water (-12‰ , Zolkos and Tank, 2019). The depleted $\delta^{18}\text{O}$ signature from FM3 persists for about two kilometers in the stream. Farther downstream, the $\delta^{18}\text{O}$ signal is similar to those in the unimpacted streams with an average of -20‰ . Outflow from RTS feature FM2 does not shift the $\delta^{18}\text{O}$ signature on the transect, i.e., the water appears to derive mostly from precipitation and active layer input, and additionally, given the dry conditions during sampling, the $\delta^{18}\text{O}$ might have been enriched due to evaporation (Craig et al., 1963). There were no rain events during the sampling period that could have shifted the water isotope signal between the sampling dates. Concentrations of DOC along the transect do not show any apparent trend, or correlation with $\delta^{18}\text{O}$, yet DOC $\delta^{13}\text{C}$ values are consistently around -26‰ ($n = 6$) when $\delta^{18}\text{O}$ values are below -20‰ (first ca. 2.5 km of transect, T1-T6) while the DOC $\delta^{13}\text{C}$ values show a somewhat larger and more depleted range (-27.2 to -28‰) when $\delta^{18}\text{O}$ values are around -20‰ (beyond ca. 2.5 km). The lowest DOC concentrations along the transect are found in the outflow from RTS feature FM2, and may reflect adsorption of DOC to particles (Kothawala et al., 2012; Littlefair et al., 2017) lowering thaw slump DOC delivery to streams on the Peel Plateau. Additionally, in the RTS runoff, particles take up such a large proportion of the volume that DOC concentrations would be even lower when one corrects for the sediment load (Shakil et al., 2020).

Our data show that along the transect mineral-specific surface area for sediments is consistently lower than for SPM, implying that finer material remains in transport whereas coarser material preferentially settles as predicted by hydrodynamic sediment transport principles. Mineral-specific surface area for streambank sediments and SPM are higher within the first two kilometers downstream from RTS feature FM3 than farther downstream (Figure 3B), whereas the median sediment

grain size shows an inverse pattern, i.e., lower grain size in the beginning of the transect than farther downstream, thus supporting the mineral-specific surface area data. This may reflect the high amount of fine-grained sediments released from the thaw slumps, and higher hydrodynamic power downstream mobilizing larger particles.

The RTS features FM3 and FM2 deliver substantial amounts of SPM and associated OC to the fluvial network. POC constitutes about 2–3% of the total suspended sediments which is a range similar to that observed in permafrost disturbed areas in the Canadian High Arctic (Lamoureux and Lafrenière, 2014). The concentrations of POC are orders of magnitude higher than those of DOC, demonstrating that most of the permafrost carbon is released in particulate form (see also Shakil et al., 2020). The overwhelming sediment delivery from the RTS features exceeds the transport capacity of the streams, which is illustrated by extremely large, and persistent debris tongue deposits comprised of 10^4 to 10^6 m³ of slump derived materials (Kokelj et al., 2020, in review), and in the decrease in POC concentrations from 600 to 2 mg L⁻¹ within the first ~2 km of the transect (see also Shakil et al., 2020). According to Kokelj et al. (2020, in review) and Shakil et al. (2020), the majority (80%) of the mobilized particulate matter of the largest RTS features affecting low-order streams accumulates on the debris tongues, thus is not immediately transported farther downstream.

Input of Fresh Organic Material and Hydrodynamic Sorting Impact Patterns in Downstream Transect

Mineral-specific surface area has been used as a tool to distinguish between sorting and degradation of organic matter in aquatic systems as riverine POC is often tightly bound (i.e., sorbed) to suspended minerals (Keil et al., 1997). It has been shown that higher mineral-specific surface area allows for a higher OC binding capacity (Keil and Mayer, 2013). Along the transect, the POC loadings (0.47–1.01 mg OC m⁻²) are within a range of typical riverine loadings (Blair and Aller, 2012), and increase downstream (Figure 4C). This may be caused by addition of fresh material (with high OC-loading) which is supported by the TOC:TN data (Supplementary Table 4). For streambank sediments, the OC loadings (0.47–0.88 mg OC m⁻²) show a more erratic pattern, but follow roughly the same trend as for POC. These POC and streambank sediment patterns contrast with general observations in larger river systems (e.g., Freymond et al., 2018) where OC loadings typically decrease downstream. We reason this contrast may either be caused by (i) an increase in the hydrodynamic power downstream that leads to additional transport of coarse particles (with low SA), but also (ii) an addition of free particulate organic matter (i.e., not associated with mineral surfaces) such as wood/plant debris downstream (with high OC).

Shift in ¹³C-DOC Values Suggests Downstream Transition From Sorption-Dominated Environment Toward Stronger Input of Fresh Material

Along the transect, the $\delta^{13}\text{C}$ values for POC and streambank sediment OC fall within a very narrow range (between -26.3

and -27.1‰), suggesting consistent OC sources or similar $\delta^{13}\text{C}$ signatures of different OC sources (Figure 5A). The latter is likely as Shakil et al. (2020) have shown that OC sources on the Peel Plateau have overlapping $\delta^{13}\text{C}$ signatures. These values are also in the same range as in Yedoma ice complex deposits in Siberia (average $\delta^{13}\text{C}$ value, $-26.3 \pm 0.67\text{‰}$; Schirrmeister et al., 2011; Vonk et al., 2012). It is however, noticeable that DOC is relatively enriched in ¹³C compared with POC and streambank sediment OC (Figure 5A) in the first ca. 2 km of the transect. This may be explained by sorption processes, as Littlefair et al. (2017) have shown to happen in the RTS-influenced streams on the Peel Plateau, where preferential sorption of the ¹³C-depleted hydrophobic fraction of DOC causes enrichment of the remaining DOC (Kaiser et al., 2001). The abrupt decrease in $\delta^{13}\text{C}$ values of DOC from -25.5 to -27.5‰ from point T6 onward (Figure 5A) implies that fresh material may be added between points T6 and T7 and further downstream, as is also suggested by the high TOC:TN ratio of SPM (Supplementary Table 4) and enriched $\delta^{18}\text{O}$ signature (Figure 3). This shift in the $\delta^{13}\text{C}$ signature of DOC may imply that input of fresh organic matter begins to dominate over sorption processes downstream of RTS features.

Suspended Sediment Load Carries the Oldest Organic Carbon

The radiocarbon data reveal that some of the old, Pleistocene permafrost-origin POC remains in suspension along the entire 12 km transect despite the rapid decline in POC concentrations in the beginning of the transect (Figure 5B). In fact, the ¹⁴C signature for POC is older than for streambank sediment OC throughout the entire transect, except for the site T6, which likely receives younger (modern) POC from a stream inflow. This trend indicates that the oldest fraction of the RTS-released material is transported predominantly in the suspended fraction, which suggests that the old Pleistocene permafrost released is finer than the modern sources (see also Bröder et al., 2021). Alternatively, fresh organic matter could be admixed with the sediments, but less so with the SPM.

The Most Recalcitrant Fraction of Organic Matter Is Transported Downstream

The dominance of refractory aromatic compounds and short-chained *n*-alkanes over the other compound classes in the RTS runoff as well as in the transect SPM and sediments, suggests that a large portion of the released permafrost carbon is not readily degradable, or that it is degraded within the scar zone prior to transport. Vancampenhout et al. (2009) found that soils in these environments may accumulate high amounts of aromatics and short- and mid-chained aliphatics, due to hampered degradation in cold climates, while in favorable conditions no relative accumulation of compounds occur. Short-chained alkanes may also derive from petrogenic sources that are known to be present in the area as shown by previous studies (e.g., Yunker et al., 2002; Hilton et al., 2015, discussed in section “Within the Slump: RTS Features as Sources of Water and Organic Matter”). Furthermore, the prominence of these refractory compounds may also indicate that they are

tightly associated with mineral particles and thus, protected from microbial degradation (Hemingway et al., 2019). However, the presence of N-containing compounds along the transect, suggest that some microbial degradation processes occur during transport. It could be that degradation mostly takes place in fresh organic matter, as we observe low (relative) abundances of polysaccharides throughout the transect that likely originate from fresh sources on the streambanks and from inflowing streams. These fresher sources are likely more prone to degradation (Bröder et al., 2021).

Along the transect, concentrations of HMW_{C27-33} *n*-alkanes (104 to 203 $\mu\text{g g}^{-1}$ OC for sediments and 57 to 345 $\mu\text{g g}^{-1}$ OC for SPM), and HMW_{C24-32} *n*-alkanoic acids (23 to 466 $\mu\text{g g}^{-1}$ OC for sediments and 88 to 1133 $\mu\text{g g}^{-1}$ OC for SPM) are lower than within the scar zone sediments. This decrease in concentrations coupled with a rapid decrease in HMW acid-to-alkane ratios (to below 1) within the first two kilometers, both for SPM and streambank sediments, suggests degradation of organic matter (Figure 9A). One could also argue that, instead of degradation, active layer contributions (with high HMW acid-to-alkane ratios and CPI values) are simply mixed with the permafrost signal that comprise a much larger part of the headwall, however, we observe a decrease in these ratios both within the scar zone as within the first transect kilometers. Similar to HMW acid-to-alkane ratios, CPI values for both streambank sediments and SPM are slightly lower along the first few kilometers of the transect than within RTS feature FM3 (see Supplementary Tables 7, 8). The increases in the HMW acid-to-alkane ratios and CPI values farther downstream along the transect (beyond T7) are likely driven by inflows from Stony Creek, unimpacted stream at N2 and RTS feature FM2, indicating addition of fresh organic matter, which is supported by the molar TOC:TN ratios (Supplementary Table 4). These results are in line with the pyrolysis data (Figure 7), suggesting that degradation and/or mixing of permafrost with more labile compounds, mainly from the active layer, occurs already within the RTS feature, while only the more recalcitrant organic matter is transported downstream. Apart from addition of fresh organic matter to the stream, erosion of debris tongues and deeply incised valleys downstream of FM2 may add recalcitrant, potentially petrogenic, organic matter to the stream. Grewer et al. (2018) have observed that active layer detachment slides in the Canadian High Arctic release dominantly recalcitrant OC to the streams. However, our *n*-alkane data show dominance of odd *n*-alkanes, especially in the HMW carbon chain lengths (C27-33) of the SPM, which is typical for biogenic sources rather than petrogenic ones (Carey et al., 1990). For the sediments, the dominance of odd *n*-alkanes is not as noticeable, and lower odd chain lengths (<C23) have higher concentrations than the HMW after the FM2 inflow (at T7) suggesting potential petrogenic input from the widespread exposure of the deep Pleistocene-aged permafrost of FM2 (headwall height ca. 25 m) along with potential bank erosion from the debris tongue. Given the evidence above, the biomarker data with low CPI values, the presence of *n*-alkanoic acids (which are commonly not found in petrogenic OC) and the dominance of odd

n-alkanes, this suggests that the organic material transported is likely a mixture of both biogenic and petrogenic sources (Supplementary Figure 1).

Streambank sediments at the beginning of the transect show high *n*-alkane CPI values and low even-to-odd *n*-alkane ratios, suggesting fresher and less degraded material than the sediments downstream, the latter exhibiting low CPI values and high even-to-odd ratios (Figure 9B). For the POC, however, no similar trend could be discerned, which may reflect addition of fresh particulate matter from the inflowing streams that confounds degradation patterns, or a lower degree of degradation in the SPM fraction of the transect (quicker transport) than in the sediment fraction (that may represent longer timescales due to deposition and re-suspension cycles). The CPI values and even-LMW-to-odd-HMW *n*-alkane ratios do not fully support the HMW acid-to-alkane ratios, which indicate degradation only within the RTS feature and in the immediate outflow. However, inflow from FM2 lowers the CPI values of *n*-alkanes likely due to addition of petrogenic carbon.

Peel Plateau organic matter released from RTS features appears to be more degraded than surface sediments in the Buor-Khaya Bay in Siberia that receive organic matter from thawing permafrost coasts and the Lena River. Surface sediments in the Buor-Khaya Bay (stations YS-13 and YS-14 in Bröder et al., 2016b) have concentrations of HMW_{C27-33} *n*-alkanes (440–537 $\mu\text{g g}^{-1}$ OC) and HMW_{C24-32} *n*-alkanoic acid (2,824–6,874 $\mu\text{g g}^{-1}$ OC) that are higher than in our transect sediments. The CPI values of our transect sediments compare to the surface sediments in the Laptev Sea: CPI values 2–10 for *n*-alkanes and 4–6 for *n*-alkanoic acids, though are also in the lower end (Bröder et al., 2016b). Similar to CPI values, HMW acid-to-alkane ratios in the Buor-Khaya Bay are in a higher range (5.3–15.2) than those along our transect (0.1–7.3), suggesting that streambank sediments on the Peel Plateau are more degraded than surface sediments in the Buor-Khaya Bay. Additionally, these differences may be due to factors such as depositional environment (marine vs. terrestrial), permafrost type (Yedoma vs. glacial tills) and degradation processes en route (submerged vs. streambank), which all likely play a role.

The Role of RTS Features on the Peel Plateau Organic Carbon Dynamics

On the Peel Plateau, Zolkos et al. (2019) have shown that the amounts of CO₂ released from the RTS-impacted streams are relatively low. Our results on the composition of thaw slump-SPM similarly suggest that a dominance of recalcitrant compounds with input from petrogenic carbon sources limits active degradation during downstream transport. Our analyses also suggest that the low CO₂ emissions that do occur (Zolkos et al., 2019) may largely result from fresh organic matter (active layer) that is either released upon slumping and degraded within the scar zone (see also Bröder et al., 2021), or is added further downstream from the surrounding active layers and fresh vegetation, and potentially degraded. While our results indicate minimal mineralization during downstream transport of POC, degradation processes within scar zones of RTS features seem more apparent (see also Bröder et al., 2021), yet mixing of

active layer with permafrost mineral soil within the scar zone, likely also plays a role. The POC is consistently older than streambank sediment OC, suggesting that the oldest, Pleistocene-aged organic carbon is transported downstream. The depletion of $\delta^{13}\text{C}$ signature of DOC downstream of RTS features suggests that addition of fresh DOC from the surrounding active layer soils likely drives the DOC dynamics farther downstream of RTS features instead of sorption to particles that Littlefair et al. (2017) have observed in the immediate runoff from RTS features. Given the fact that the number and size of RTS features on the Peel Plateau are increasing (Kokelj et al., 2015), degradation of released OC within scar zones may become more important. The increasing size of the RTS features also increases depth of the scar concavity (Kokelj et al., 2020, in review), which raises the volume of sediment that could be mobilized to the stream system, and the depths within the stratigraphic profile from which they are derived. However, as deepening will likely expose and mobilize predominantly recalcitrant permafrost organic matter, its climate feedback may remain relatively small. Additionally, the climate impact of RTS features over longer time scales might change if the increased solute load changes the in stream physico-chemical conditions, such as pH, leading to potential release of mineral-bound organic carbon (Opfergelt, 2020). These results of RTS impact on fluvial systems on the Peel Plateau may be applicable to other ice-marginal regions in North-America (Kokelj et al., 2017b - see map) that are underlain by ice-rich permafrost and comprise of glacial sediments, indicating that more studies on POC composition and degradability are needed to be able to better understand implications on a wider scale.

CONCLUSION

In this study, we addressed bulk geochemical and sedimentological properties as well as the (macro)molecular composition of suspended and streambank sediments released from two large RTS features and their downstream transport on the Peel Plateau. Pleistocene-aged permafrost POC is traceable for > 10 km downstream, suggesting that RTS features, which are increasing in size and number on the Peel Plateau, impact watersheds on a larger scale by adding old POC to the stream system. However, the mobilized POC is dominated by recalcitrant compounds, such as aromatics, which suggests that RTS activity on the Peel Plateau mostly conveys a large amount of permafrost OM to sites of reburial, with limited (potential for) degradation during fluvial transport. Our results (along with Bröder et al., 2021) suggest that ongoing degradation is mostly confined to the scar zone of the RTS feature itself and in the immediate runoff. The most labile organic matter fraction seems to mainly derive from the active layer rather than from old-Pleistocene permafrost. The contribution of petrogenic carbon released from RTS features may become more abundant in the future as the RTS features deepen and expose more Pleistocene-aged permafrost. Glacial ice-margins, such as the Peel Plateau, are particularly susceptible to thermokarst processes thus a better understanding of these landscapes and the complexity associated with the mobilization and mixing of

materials before further transport and their re-deposition on debris tongues is crucial for deciphering their potential climate impact on longer timescales.

DATA AVAILABILITY STATEMENT

The original contributions presented in the study are included in the article/**Supplementary Material**, further inquiries can be directed to the corresponding author/s.

AUTHOR CONTRIBUTIONS

JV, LB, and KK designed the study. KK, LB, SS, SZ, and ST collected the samples. NH and TE provided the radiocarbon analyses. KK and BD analyzed the samples for py-GCMS. KK carried out rest of the laboratory work with support from TT and LB, and wrote the manuscript with contributions from all the co-authors. All authors contributed to the article and approved the submitted version.

FUNDING

This study was funded with a European Research Council Starting Grant to JV (THAWSOME #676982). ST, SS, and SZ received funds from the Campus Alberta Innovates Program, the Natural Sciences and Engineering Research Council of Canada (NSERC, #444873 and #430696), and the Polar Continental Shelf Program (#617-17).

ACKNOWLEDGMENTS

We would like to thank the staff of the Aurora Research Institute (ARI) for their field support and providing laboratory facilities, Erin MacDonald and Rosemin Nathoo for their help in the field as well as Georgina Neyando, Andrew Koe, and Dempster Colin for wildlife monitoring, Jorien Schoorl-Smits for the laboratory analyses at the University of Amsterdam, Charlotte van der Nagel for her contribution to the laboratory work at the Vrije Universiteit Amsterdam, and Laboratory for Ion Beam Physics at ETH Zürich for AMS support. We are also grateful to Hugues Lantuit, George Tanski, and Dirk Jong for their support in the field. We would also like to acknowledge that this study was conducted within the Gwich'in Settlement region. This publication is related to NWT Geological Survey Contribution #0137. Finally, we would also like to thank the editor EJ and the two reviewers whose comments helped to improve this manuscript.

SUPPLEMENTARY MATERIAL

The Supplementary Material for this article can be found online at: <https://www.frontiersin.org/articles/10.3389/feart.2021.642675/full#supplementary-material>

REFERENCES

- Abbott, B. W., Jones, J. B., Godsey, S. E., Larouche, J. R., and Bowden, W. B. (2015). Patterns and persistence of hydrologic carbon and nutrient export. *Biogeosciences* 12, 3725–3740. doi: 10.5194/bg-12-3725-2015
- Biskaborn, B. K., Smith, S. L., Noetzi, J., Matthes, H., Vieira, G., Streletskiy, D. A., et al. (2019). Permafrost is warming at a global scale. *Nat. Commun.* 10:264.
- Blair, N. E., and Aller, R. C. (2012). The fate of terrestrial organic carbon in the marine environment. *Ann. Rev. Mar. Sci.* 4, 401–423. doi: 10.1146/annurev-marine-120709-142717
- Bray, E. E., and Evans, E. D. (1961). Distribution of n-paraffins as a clue to recognition of source beds. *Geochim. Cosmochim. Acta* 22, 2–15. doi: 10.1016/0016-7037(61)90069-2
- Bröder, L., Keskitalo, K., Zolkos, S., Shakil, S., Tank, S. E., Kokelj, S. V., et al. (2021). Preferential export of permafrost-derived organic matter as retrogressive thaw slumping intensifies. *Environ. Res. Lett.* doi: 10.1088/1748-9326/abee4b
- Bröder, L., Tesi, T., Andersson, A., Eglinton, T. I., Semiletov, I. P., Dudarev, O. V., et al. (2016a). Historical records of organic matter supply and degradation status in the East Siberian Sea. *Org. Geochem.* 91, 16–30. doi: 10.1016/j.orggeochem.2015.10.008
- Bröder, L., Tesi, T., Salvadó, J. A., Semiletov, I. P., Dudarev, O. V., and Gustafsson, Ö (2016b). Fate of terrigenous organic matter across the Laptev Sea from the mouth of the Lena River to the deep sea of the Arctic interior. *Biogeosciences* 13, 5003–5019. doi: 10.5194/bg-13-5003-2016
- Carey, J. H., Ongley, E. D., and Nagy, E. (1990). Hydrocarbon transport in the Mackenzie River, Canada. *Sci. Total Environ.* 9, 69–88. doi: 10.1016/0048-9697(90)90231-i
- Cory, R. M., Crump, B. C., Dobkowski, J. A., and Kling, G. W. (2013). Surface exposure to sunlight stimulates CO₂ release from permafrost soil carbon in the Arctic. *PNAS* 110, 3429–3434. doi: 10.1073/pnas.1214104110
- Craig, H., Gordon, L., and Horibel, Y. (1963). Isotopic exchange effects in the evaporation of water. *J. Geophys. Res.* 68, 5079–5087. doi: 10.1029/jz068i017p05079
- Dai, X. Y., White, D., and Ping, C. L. (2002). Comparing bioavailability in five Arctic soils by pyrolysis-gas chromatography / mass spectrometry. *J. Anal. Appl. Pyrolysis* 62, 249–258. doi: 10.1016/S0165-2370(01)00123-1
- Duk-Rodkin, A., and Hughes, O. L. (1992). *Surficial Geology, Fort McPherson-Bell River, Yukon-Northwest Territories*. Canada: Geological Survey of Canada
- Dyke, A. S., Andrews, J. T., Clark, P. U., England, J. H., Miller, G. H., Shaw, J., et al. (2002). The Laurentide and Innuitian ice sheets during the Last Glacial Maximum, *quat. Sci. Rev.* 21, 9–31. doi: 10.1016/S0277-3791(01)00095-6
- Eglinton, G., and Hamilton, R. J. (1967a). Leaf epicuticular waxes. *Science* 156, 1322–1335. doi: 10.1126/science.156.3780.1322
- Eglinton, G., and Hamilton, R. J. (1967b). “The distribution of alkanes,” in *Comparative Phytochemistry*, ed. T. Swain (London: Academic Press), 57–78.
- Environment Canada (2019). *Canadian Climate Normals 1981-2010. Station Fort McPherson*. Available online at: https://climate.weather.gc.ca/climate_normals/ (accessed May 11th, 2020).
- Ewing, S. A., Donnell, J. A. O., Aiken, G. R., Butler, K. D., Butman, D., Windhammyers, L., et al. (2015). Long-term anoxia and release of ancient, labile carbon upon thaw of Pleistocene permafrost. *geophys. Res. Lett.* 42, 10730–10738.
- Farquharson, L. M., Romanovsky, V. E., Cable, W. L., Walker, D. A., Kokelj, S. V., and Nicolsky, D. (2019). Climate change drives widespread and rapid thermokarst development in very cold permafrost in the Canadian high Arctic. *Geophys. Res. Lett.* 46, 6681–6689. doi: 10.1029/2019gl082187
- Freymond, C. V., Ku, N., Lupker, M., Plo, M., Blattmann, T. M., Filip, F., et al. (2018). Evolution of biomolecular loadings along a major river system. *Geochim. Cosmochim. Acta.* 223, 389–404. doi: 10.1016/j.gca.2017.12.010
- Freymond, C. V., Peterse, F., Fischer, L. V., Filip, F., Giosan, L., and Eglinton, T. I. (2017). Branched GDGT signals in fluvial sediments of the Danube river basin: method comparison and longitudinal evolution. *Org. Geochem.* 103, 88–96. doi: 10.1016/j.orggeochem.2016.11.002
- Greuer, D. M., Lafrenière, M. J., Lamoureux, S. F., and Simpson, M. J. (2018). Spatial and temporal shifts in fluvial sedimentary organic matter composition from a high Arctic watershed impacted by localized slope disturbances. *Org. Geochem.* 123, 113–125. doi: 10.1016/j.orggeochem.2018.07.004
- Grimalt, J., and Albaigés, J. (1987). Sources and occurrence of C₁₂C₂₂ n-alkane distributions with even carbon-number preference in sedimentary environments. *Geochim. Cosmochim. Acta* 51, 1379–1384. doi: 10.1016/0016-7037(87)90322-x
- Guo, L., Lehner, J. K., White, D. M., and Garland, D. S. (2003). Heterogeneity of natural organic matter from the Chena River, Alaska. *Water Res.* 37, 1015–1022. doi: 10.1016/S0043-1354(02)00443-8
- Guo, L., White, D. M., Xu, C., and Santschi, P. H. (2009). Chemical and isotopic composition of high-molecular-weight dissolved organic matter from the Mississippi River plume. *Mar. Chem.* 114, 63–71. doi: 10.1016/j.marchem.2009.04.002
- Haghipour, N., Ausin, B., Usman, M. O., Ishikawa, N., Wacker, L., Welte, C., et al. (2019). Compound-specific radiocarbon analysis by elemental analyzer-accelerator mass spectrometry: precision and limitations. *Anal. Chem.* 91, 2042–2049. doi: 10.1021/acs.analchem.8b04491
- Hemingway, J. D., Rothman, D. H., Grant, K. E., Rosengard, S. Z., Eglinton, T. I., Derry, L. A., et al. (2019). Mineral protection regulates long-term global preservation of natural organic carbon. *Nature* 570, 228–231. doi: 10.1038/s41586-019-1280-6
- Hilton, R. G., Galy, V., Gaillardet, J., Dellinger, M., Bryant, C., O’Regan, M., et al. (2015). Erosion of organic carbon in the Arctic as a geological carbon dioxide sink. *Nature* 524, 84–87. doi: 10.1038/nature14653
- Hugelius, G., Strauss, J., Zubrzycki, S., Harden, J. W., Schuur, E. A. G., Ping, C., et al. (2014). Estimated stocks of circum-polar permafrost carbon with quantified. *Biogeosciences* 11, 6573–6593. doi: 10.5194/bg-11-6573-2014
- IPCC (2013). “Climate change 2013: the physical science basis,” in *Contribution of Working Group I to the 5th Assessment Report of the Intergovernmental Panel on Climate Change*, eds T. F. Stocker, D. Qin, G.-K. Plattner, M. Tignor, S. K. Allen, J. Boschung, (Cambridge: Cambridge University Press).
- Jasechko, S. (2019). Global isotope hydrogeology—review. *Rev. Geophys.* 57, 835–965.
- Kaiser, K., Guggenberger, G., and Zech, W. (2001). Isotopic fractionation of dissolved organic carbon in shallow forest soils as affected by sorption. *Eur. J. Soil Sci.* 52, 585–597. doi: 10.1046/j.1365-2389.2001.00407.x
- Keil, R. G., and Mayer, L. M. (2013). “Mineral matrices and organic matter,” in *Treatise on Geochemistry: Second Edition*, eds H. E. Holland and K. K. Turekian (Elsevier Ltd), 337–359. doi: 10.1016/B978-0-08-095975-7.01024-x
- Keil, R. G., Mayer, L. M., Quay, P. D., Richey, J. E., and Hedges, J. I. (1997). Loss of organic matter from riverine particles in deltas. *Geochim. Cosmochim. Acta* 61, 1507–1511. doi: 10.1016/S0016-7037(97)00044-6
- Kokelj, S. V., and Jorgenson, M. T. (2013). Advances in thermokarst research. *Permafrost Periglacial Process.* 24, 108–119. doi: 10.1002/ppp.1779
- Kokelj, S. V., Kokoszka, J., van der Sluijs, J., Rudy, A. C. A., Tunnicliffe, J., Shakil, S., et al. (2020). *Permafrost thaw Couples Slopes with Downstream Systems and Effects Propagate Through Arctic Drainage Networks*. Available online at: <https://doi.org/10.5194/tc-2020-218> (accessed September 29, 2020).
- Kokelj, S. V., Lacelle, D., Lantz, T. C., Tunnicliffe, J., Malone, L., Clark, I. D., et al. (2013). Thawing of massive ground ice in mega slumps drives increases in stream sediment and solute flux across a range of watershed scales. *J. Geophys. Res. Earth Surf.* 118, 681–692. doi: 10.1002/jgrf.20063
- Kokelj, S. V., Lantz, T. C., Tunnicliffe, J., Segal, R., and Lacelle, D. (2017b). Climate-driven thaw of permafrost preserved glacial landscapes, northwestern Canada. *Geology* 45, 371–374. doi: 10.1130/g38626.1
- Kokelj, S. V., Tunnicliffe, J., and Lacelle, D. (2017a). “The Peel Plateau of northwestern Canada: an ice-rich hummocky moraine landscape in transition,” in *Landscapes and Landforms of Western Canada*, ed. O. Slaymaker (Cham: Springer), 381–393.
- Kokelj, S. V., Tunnicliffe, J., Lacelle, D., Lantz, T. C., Chin, K. S., and Fraser, R. (2015). Increased precipitation drives mega slump development and destabilization of ice-rich permafrost terrain, northwestern Canada. *Glob. Planet. Change* 129, 56–68. doi: 10.1016/j.gloplacha.2015.02.008
- Kothawala, D. N., Roehm, C., Blodau, C., and Moore, T. R. (2012). Selective adsorption of dissolved organic matter to mineral soils. *Geoderma* 189–190, 334–342. doi: 10.1016/j.geoderma.2012.07.001
- Lacelle, D., Brooker, A., Fraser, R. H., and Kokelj, S. V. (2015). Distribution and growth of thaw slumps in the Richardson mountains-Peel Plateau region, northwestern Canada. *Geomorphology* 235, 40–51. doi: 10.1016/j.geomorph.2015.01.024

- Lacelle, D., Fontaine, M., Pellerin, A., Kokelj, S. V., and Clark, I. D. (2019). Legacy of Holocene landscape changes on soil biogeochemistry: a perspective from paleo-active layers in Northwestern Canada. *J. Geophys. Res. Biogeosci.* 124, 2662–2679. doi: 10.1029/2018jg004916
- Lacelle, D., Lauriol, B., Zazula, G., Ghaleb, B., Utting, N., and Clark, I. D. (2013). Timing of advance and basal condition of the Laurentide Ice Sheet during the last glacial maximum in the Richardson mountains, NWT. *Quat. Res.* 80, 274–283. doi: 10.1016/j.yqres.2013.06.001
- Lamoureux, S. F., and Lafrenière, M. J. (2014). Seasonal fluxes and age of particulate organic carbon exported from Arctic catchments impacted by localized permafrost slope disturbances. *Environ. Res. Lett.* 9:045002. doi: 10.1088/1748-9326/9/4/045002
- Lewkowicz, A. G., and Way, R. G. (2019). Extremes of summer climate trigger thousands of thermokarst landslides in a high arctic environment. *Nat. Commun.* 10:1329.
- Littlefair, C. A., and Tank, S. E. (2018). Biodegradability of thermokarst carbon in a till-associated, glacial margin landscape: the case of the Peel Plateau, NWT, Canada. *J. Geophys. Res. Biogeosciences.* 123, 3293–3307. doi: 10.1029/2018jg004461
- Littlefair, C. A., Tank, S. E., and Kokelj, S. V. (2017). Retrogressive thaw slumps temper dissolved organic carbon delivery to streams of the Peel Plateau, NWT, Canada. *Biogeosciences* 14, 5487–5505. doi: 10.5194/bg-14-5487-2017
- Malone, L., Lacelle, D., Kokelj, S., and Clark, I. D. (2013). Impacts of hillslope thaw slumps on the geochemistry of permafrost catchments (Stony Creek watershed, NWT, Canada). *Chem. Geol.* 356, 38–49. doi: 10.1016/j.chemgeo.2013.07.010
- Mann, P. J., Eglinton, T. I., McIntyre, C. P., Zimov, N., Davydova, A., Vonk, J. E., et al. (2015). Utilization of ancient permafrost carbon in headwaters of Arctic fluvial networks. *Nat. Commun.* 6:7856.
- Matiasek, S. J., and Hernes, P. J. (2019). The chemical fingerprint of solubilized organic matter from eroded soils and sediments. *Geochim. Cosmochim. Acta* 267, 92–112. doi: 10.1016/j.gca.2019.09.016
- Meredith, M., Sommerkorn, M., Cassotta, S., Derksen, C., Ekaykin, A., Hollowed, A., et al. (2019). “Polar Regions,” in IPCC Special Report on the Ocean and Cryosphere in a Changing Climate, eds H. O. Portner, D. O. Portner, D. C. Roberts, and V. Masson-Delmotte (Geneva: IPCC).
- Meyers, P. A. (1994). Preservation of elemental and isotopic source identification of sedimentary organic matter. *Chem. Geol.* 114, 289–302. doi: 10.1016/0009-2541(94)90059-0
- O’Neill, H. B., Burn, C. R., Kokelj, S. V., and Lantz, T. C. (2015). Warm tundra: atmospheric and near-surface ground temperature inversions across an alpine treeline in continuous permafrost, Western Arctic, Canada. *Permafrost. Periglac. Process.* 26, 103–118. doi: 10.1002/ppp.1838
- Olefeldt, D., Goswami, S., Grosse, G., Hayes, D., Hugelius, G., Kuhry, P., et al. (2016). Circumpolar distribution and carbon storage of thermokarst landscapes. *Nat. Commun.* 7:13043.
- Opfergelt, S. (2020). The next generation of climate model should account for the evolution of mineral-organic interactions with permafrost thaw. *Environ. Res. Lett.* 15:091003. doi: 10.1088/1748-9326/ab9a6d
- Plaza, C., Pegoraro, E., Bracho, R., Celis, G., Crummer, K. G., Hutchings, J. A., et al. (2019). Direct observation of permafrost degradation and rapid soil carbon loss in tundra. *Nat. Geosci.* 12, 627–631. doi: 10.1038/s41561-019-0387-6
- Porter, C., Morin, P., Howat, I., Noh, M.-J., Bates, B., Peterman, K., et al. (2018). *ArcticDEM*. Available online at: <https://doi.org/10.7910/DVN/OHHUKH>, Harvard Dataverse, V1, (accessed January 24, 2020).
- Rudy, A. C. A., Lamoureux, S. F., Kokelj, S. V., Smith, I. R., and England, J. H. (2017). Accelerating thermokarst transforms ice-cored terrain triggering a downstream cascade to the ocean. *Geophys. Res. Lett.* 44:11:087.
- Sánchez-García, L., Vonk, J. E., Charkin, A. N., Kosmach, D., Dudarev, O. V., Semiletov, I. P., et al. (2014). Characterisation of three regimes of collapsing arctic ice complex deposits on the SE Laptev Sea coast using biomarkers and dual carbon isotopes. *Permafrost. Periglac. Process.* 25, 172–183. doi: 10.1002/ppp.1815
- Schirrmeister, L., Kunitsky, V., Grosse, G., Wetterich, S., Meyer, H., Schwaborn, G., et al. (2011). Sedimentary characteristics and origin of the late pleistocene ice complex on north-east Siberian Arctic coastal lowlands and islands - a review. *Quat. Int.* 241, 3–25. doi: 10.1016/j.quaint.2010.04.004
- Schmidt, M. W. I., Knicker, H., and Kögel-Knabner, I. (2000). Organic matter accumulating in Aeh and Bh horizons of a Podzol - chemical characterization in primary organo-mineral associations. *Org. Geochem.* 31, 727–734. doi: 10.1016/S0146-6380(00)00045-0
- Schuur, E. A. G., McGuire, A. D., Schädler, C., Grosse, G., Harden, J. W., Hayes, D. J., et al. (2015). Climate change and the permafrost carbon feedback. *Nature* 520, 171–179.
- Segal, R. A., Lantz, T. C., and Kokelj, S. V. (2016). Acceleration of thaw slump activity in glaciated landscapes of the Western Canadian Arctic. *Environ. Res. Lett.* 11:034025. doi: 10.1088/1748-9326/11/3/034025
- Shakil, S., Tank, S. E., Kokelj, S. V., Vonk, J. E., and Zolkos, S. (2020). Particulate dominance of organic carbon mobilization from thaw slumps on the Peel Plateau, NT: Quantification and implications for stream systems and permafrost carbon release. *Environ. Res. Lett.* 15:114019. doi: 10.1088/1748-9326/abac36
- Sparkes, R. B., Selver, A. D., Gustafsson, Ö, Semiletov, I. P., Haghypour, N., and Wacker, L. (2016). Macromolecular composition of terrestrial and marine organic matter in sediments across the East Siberian Arctic Shelf. *Cryosphere* 10, 2485–2500. doi: 10.5194/tc-10-2485-2016
- Strauss, J., Schirrmeister, L., Grosse, G., Fortier, D., Hugelius, G., Knoblauch, C., et al. (2017). Earth-science reviews deep yedoma permafrost: a synthesis of depositional characteristics and carbon vulnerability. *Earth Sci. Rev.* 172, 75–86. doi: 10.1016/j.earscirev.2017.07.007
- Synal, H. A., Stocker, M., and Suter, M. (2007). MICADAS: a new compact radiocarbon AMS system. *Nucl. Instrum. Methods Phys. Res.* 259, 7–13. doi: 10.1016/j.nimb.2007.01.138
- Tank, S. E., Vonk, J. E., Walvoord, M. A., McClelland, J. W., Laurion, I., and Abbott, B. W. (2020). Landscape matters: predicting the biogeochemical effects of permafrost thaw on aquatic networks with a state factor approach. *Permafrost. Periglac. Process.* 31, 358–370. doi: 10.1002/ppp.2057
- Tanski, G., Lantuit, H., Ruttner, S., Knoblauch, C., Radosavljevic, B., Strauss, J., et al. (2017). Transformation of terrestrial organic matter along thermokarst-affected permafrost coasts in the Arctic. *Sci. Total Environ.* 58, 434–447. doi: 10.1016/j.scitotenv.2016.12.152
- Textor, S. R., Wickland, K. P., Podgorski, D. C., Johnston, S. E., and Spencer, R. G. M. (2019). Dissolved organic carbon turnover in permafrost-influenced watersheds of interior Alaska: molecular insights and the priming effect. *Front. Earth Sci.* 7:275.
- Turetsky, M. R., Abbott, B. W., Jones, M. C., Anthony, K. W., Olefeldt, D., Schuur, E. A. G., et al. (2020). Carbon release through abrupt permafrost thaw. *Nat. Geosci.* 13, 138–143. doi: 10.1038/s41561-019-0526-0
- van der Sluijs, J., Kokelj, S. V., Fraser, R. H., Tunnicliffe, J., and Lacelle, D. (2018). Permafrost terrain dynamics and infrastructure impacts revealed by UAV photogrammetry and thermal imaging. *Remote Sens.* 10:1734. doi: 10.3390/rs10111734
- van Dongen, B. E., Semiletov, I., and Weijers, J. W. H. (2008). Contrasting lipid biomarker composition of terrestrial organic matter exported from across the Eurasian Arctic by the five great Russian Arctic rivers. *Global Biogeochem. Cycles* 22, 1–14. doi: 10.1016/j.marchem.2008.07.001
- Van Heemst, J. D. H., Van Bergen, P. F., Stankiewicz, B. A., and De Leeuw, J. W. (1999). Multiple sources of alkylphenols produced upon pyrolysis of DOM, POM and recent sediments. *J. Anal. Appl. Pyrolysis.* 52, 239–256. doi: 10.1016/S0165-2370(99)00047-9
- Vancampenhout, K., Wouters, K., De Vos, B., Buurman, P., Swennen, R., and Deckers, J. (2009). Differences in chemical composition of soil organic matter in natural ecosystems from different climatic regions - a pyrolysis-GC/MS study. *Soil Biol. Biochem.* 41, 568–579. doi: 10.1016/j.soilbio.2008.12.023
- Vonk, J. E., Mann, P. J., Davydov, S., Davydova, A., Spencer, R. G. M., Schade, J., et al. (2013). High biolability of ancient permafrost carbon upon thaw. *Geophys. Res. Lett.* 40, 2689–2693. doi: 10.1002/grl.50348
- Vonk, J. E., Sánchez-García, L., van Dongen, B. E., Alling, V., Kosmach, D., Charkin, A., et al. (2012). Activation of old carbon by erosion of coastal and subsea permafrost in Arctic Siberia. *Nature* 489, 137–140. doi: 10.1038/nature11392
- Vonk, J. E., Tank, S. E., Bowden, W. B., Laurion, I., Vincent, W. F., Alekseychik, P., et al. (2015b). Reviews and syntheses: effects of permafrost thaw on Arctic aquatic ecosystems. *Biogeosciences* 12, 7129–7167. doi: 10.5194/bg-12-7129-2015

- Vonk, J. E., Tank, S. E., Mann, P. J., Spencer, R. G. M., Treat, C. C., Striegl, R. G., et al. (2015a). Biodegradability of dissolved organic carbon in permafrost soils and aquatic systems: a meta-analysis. *Biogeosciences* 12, 6915–6930. doi: 10.5194/bg-12-6915-2015
- Xu, C., Guo, L., Ping, C., and White, D. M. (2009). Chemical and isotopic characterization of size-fractionated organic matter from cryoturbated tundra soils, northern Alaska. *J. Geophys. Res.* 114:G03002.
- Yunker, M. B., Backus, S. M., Graf Pannatier, E., Jeffries, D. S., and Macdonald, R. W. (2002). Sources and significance of alkane and PAH hydrocarbons in Canadian Arctic Rivers. *Estuar. Coast. Shelf Sci.* 55, 1–31. doi: 10.1006/ecss.2001.0880
- Zazula, G. D., MacKay, G., Andrews, T. D., Shapiro, B., Letts, B., and Brock, F. (2009). A late Pleistocene steppe bison (*Bison priscus*) partial carcass from Tsiigehtchic, Northwest Territories, Canada. *Quat. Sci. Rev.* 28, 2734–2742. doi: 10.1016/j.quascirev.2009.06.012
- Zimov, S. A., Schuur, E. A. G., and Stuart Chapin, F. (2006). Permafrost and the global carbon budget. *Science* 312, 1612–1613. doi: 10.1126/science.1128908
- Zolkos, S., and Tank, S. E. (2019). Permafrost Geochemistry and Retrogressive Thaw Slump Morphology (Peel Plateau, Canada). v. 1.0 (2017-2017). Nordicana D45. Available online at: <https://doi.org/10.5885/45573XD-28DD57D553F14BF0> (accessed June 10, 2020).
- Zolkos, S., Tank, S. E., and Kokelj, S. V. (2018). Mineral weathering and the permafrost carbon-climate feedback. *Geophys. Res. Lett.* 45, 9623–9632. doi: 10.1029/2018gl078748
- Zolkos, S., Tank, S. E., Striegl, R. G., and Kokelj, S. V. (2019). Thermokarst effects on carbon dioxide and methane fluxes in streams on the Peel Plateau (NWT, Canada). *J. Geophys. Res. Biogeosci.* 124, 1781–1798. doi: 10.1029/2019jg005038

Conflict of Interest: The authors declare that the research was conducted in the absence of any commercial or financial relationships that could be construed as a potential conflict of interest.

Copyright © 2021 Keskitalo, Bröder, Shakil, Zolkos, Tank, van Dongen, Tesi, Haghypour, Eglinton, Kokelj and Vonk. This is an open-access article distributed under the terms of the Creative Commons Attribution License (CC BY). The use, distribution or reproduction in other forums is permitted, provided the original author(s) and the copyright owner(s) are credited and that the original publication in this journal is cited, in accordance with accepted academic practice. No use, distribution or reproduction is permitted which does not comply with these terms.